Temple University

College of Engineering

Bioengineering

Final Design

Partial Gravity Bioreactor

Presented By: Team #13

Dmitry M Hackel *Irene Bui*

Jake Fisher *Zenub Abouzid*

Supervised By:

Dr. Yah-el Har-el & Dr. Peter Lelkes

1 0 – 0 5 – 2 0 2 5

Acknowledgment

We want to extend our most profound appreciation to the following individuals and organizations who have contributed to the completion of this project:

- Dr. Yar-el Har-el, for providing guidance and feedback throughout the course of this project through her professor and advisor roles.

- Dr. Peter Lelkes, a subject matter expert and our advisor, for providing valuable information and resources for our research.

- Dr. Jonathan Gerstenhaber, for providing valuable information, previous prototypes, and ideas that paved the way for the prototype.

- Brian Amin and Matthew Short, a previous team who completed a similar topic, for giving us the time to explain their prototype in more depth.

- Temple University, for providing access to their machines, labs, and space.

Additionally, we would like to express our gratitude to all those who have supported us in ways both seen and unseen. Without your contributions and presence, this project would not have been possible.

Thank you.

Abstract

The progress of human exploration to space, the Moon, and Mars is not considered safe because of the limited understanding of how partial gravity impacts human cells. This issue has not been fully addressed due to cost limitations and the difficulty of accurately simulating partial gravity on Earth. This project focused on developing a validated prototype for a partial gravity bioreactor. By successfully simulating the mathematical model and conducting tests to validate the prototype visually, the accuracy between the models can be determined.

Table of Contents

List of Acronyms/Abbreviations

MOND	Modified Newtonian Dynamics
ACME	Advanced Combustion via Microgravity Experiments
NASA	The National Aeronautics and Space Administration
ISS	International Space Station
$0G$	Zero Gravity
μG	Microgravity
$\frac{1}{6}G$	Lunar Gravity
$\frac{3}{8}G$	Martian Gravity
$1G$	Earth Gravity
RWV	Rotating Wall Vessel
UNSDG	United Nations Sustainable Development Goals
SDG	Sustainable Development Goals
DGD	Degree of Gravity Dispersion
RGP	Reduced Gravity Paradigm
STLV	Slow-Turning Lateral Vessel
HARV	High Aspect Ratio Vessel
MAGICIAN	Mars Artificial Gravity Habitat with Centrifugation

List of Figures

List of Tables

1. Problem Statement

1.1 Overall Objective

Since the 1960s, space exploration has yielded intriguing discoveries that continue to unfold over time. Yuri Gagarin became the first human in space in 1961, paving the way for thousands of astronauts and cosmonauts to follow him as the years passed [1]. Various theories have been proposed based on space, including the Croatian Barrel Theory, which explains how the solar system, stars, and other celestial bodies formed [2][3]. In 2002, research refuted the theory that gravity alone governs the universe, as it could not explain specific astronomical observations [4]. Sanders and McGaugh modified Newtonian gravity as an alternative to cosmic dark matter, known as Modified Newtonian Dynamics (MOND), correlating a relationship between the acceleration from Newtonian gravity and the observed acceleration at any radius in a galaxy [5][6].

Exploring space not only reveals discoveries beyond our planet, but it also uncovers truths that enhance and govern our lives. Advanced Combustion via Microgravity Experiments (ACME) investigates fuel efficiency and pollutant production in combustion under microgravity conditions on Earth [7]. One of their investigations, Flame Design, studied the quantity of soot produced under different flame conditions [7]. Such a discovery could lead to more efficient combustion, reducing pollution on Earth [7]. In the ongoing Moon exploration, researchers found that the Moon's gravity affects Earth's tides, plant growth, animal behavior, and agricultural practices [8]. Moreover, models have shown that the Earth-Moon coupled magnetospheres provide a buffer against the solar wind, allowing for a reduction in Earth's atmospheric loss to space [9]. The National Aeronautics and Space Administration (NASA) has been exploring Mars for over sixty years to decide whether it is or was a habitable world [10]. Since Mars is the most similar planet to Earth in the Solar System, understanding its surface and evolution is crucial for preparing for future human exploration [11]. With evidence suggesting that Mars was once full of water, warmer, and had a thicker atmosphere, it is highly likely that Mars could be a habitable environment [11].

Traveling beyond Earth's atmosphere to investigate potential extraterrestrial life entails considerable risks and substantial financial investment. Considering that human physiology is heavily dependent on gravity, any significant fluctuations in gravitational force may lead to serious health issues [12]. Gravity, as a vector quantity, influences all objects by determining their weight relative to their mass [13]. Biological organisms respond to environmental stimuli—including gravity—by developing unique morphological traits, physiological characteristics, behaviors, and habitat preferences [13]. The sensitivity of organisms to changes in gravity increases with their size and mass, with single cells enduring exposures up to 10^5G and humans tolerating gravitational forces of 4-5G [13]. At the cellular level, cells comprise organelles, each with mass and thus subject to gravitational forces [14]. Variations in gravitational vectors could disrupt cellular homeostasis, affecting structural integrity, composition, and orientation, such as the cytoskeleton, which maintains cellular shape [14]. Additionally, numerous studies have documented genes exhibiting sensitivity to gravity alterations, including modifications in cytoskeletal gene expression pathways and gene inhibition following microgravity exposure [15][16]. In the absence of gravity, cellular growth pathways shift, and metabolic processes adapt due to changes in reactive oxygen species levels [17][18]. Furthermore,

cellular adaptation to gravity is crucial for tissue adaptation, as bones contain osteocytes that sense and respond to varying gravitational loads [13].

Such cellular changes impact the entire human system. Astronauts exposed to microgravity undergo physiological deconditioning in systems sensitive to mechanical loading, including the cardiovascular, pulmonary, and musculoskeletal systems [19]. To mitigate these effects, International Space Station (ISS) crew members engage in rigorous exercise; however, despite extensive physical activity, astronauts still return from their six-month ISS missions exhibiting decreased calf muscle volume and strength, loss of bone mineral density, and reduced peak oxygen uptake [20][21][22][23].

Given that, it is highly unethical to send people into space without understanding the effects of gravitational changes on the body. This paper discusses a validated proposed prototype of a device that cultures cells under the influence of partial gravity and microgravity, enabling the correlation of specific cell behaviors with gravitational differences.

1.2 Background

Understanding the effects of partial gravity on humans is less extensively studied due to the high costs associated with conducting tests in partial or microgravity environments. Between 1960 and 1973, the research experience and studies gained during the Apollo missions—focused on lunar exploration—provided valuable insights into the diverse effects of partial gravity on the human musculoskeletal, cardiovascular, and respiratory systems, employing either microgravity or Earth's gravity as controls [24][25]. However, the Apollo missions cost approximately $25.4 billion in 1969, equivalent to roughly $217 billion in 2024 [26]. Following these missions, despite the lack of subsequent lunar landings, the failures in early missions facilitated advancements in spacecraft design, including the incorporation of additional protective layers and the development of new, safer materials, as well as the integration of computer systems for troubleshooting purposes [27]. In 2019, the health impacts of a year-long space mission were examined at both the molecular and psychological levels by comparing the DNA sequences of twin brothers, Mark and Scott Kelly, with Mark Kelly remaining on Earth serving as the control, and Scott Kelly participating in spaceflight [28][29]. The study revealed that extensive changes in multisystem and gene expression occur during spaceflight [28]. Astronauts may face risks including mitochondrial dysfunction, immunological stress, vascular modifications, fluid shifts, and cognitive performance decline, as well as alterations in telomere length, gene regulation, and genome integrity [28].

Given the expenses and decommissioning of the ISS, researchers endeavored to replicate partial gravity conditions on Earth, such as employing a pulley-spring system to simulate partial gravity for rodents (refer to **Error! Reference source not found.**) [23][30]. However, a limitation of the apparatus was that only the tail was suspended rather than the entire body, resulting in a weight shift within the rodent's body and thus failing to provide a truly accurate simulation [30].

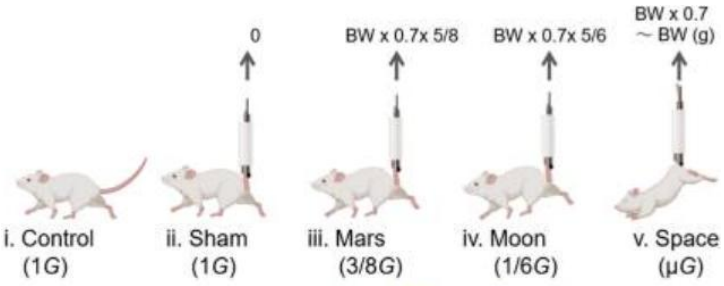

Figure 1. Experimental Design for Simulated Partial Gravity Apparatus for Rats
The figure shows the groups of experimental rats with the Control group ($1G$) (i); the sham group with SA ($1G$) (ii); the Mars group ($\frac{3}{8}G$) (iii); the Moon group ($\frac{1}{6}G$) (iv); and the interplanetary space (μG) group (v) [18].

The effects of gravity on an object may manifest as either displacement or deformation [31]. Microgravity creates distinctive environments conducive to cell growth, whereas partial gravity (such as on the Moon and Mars) may yield markedly different effects [32]. To comprehensively understand the concepts related to partial gravity apparatuses, it is imperative to distinguish between zero gravity, gravity, microgravity, and partial gravity. Gravity is an abstract phenomenon that can be quantified; however, its fundamental cause remains unknown [33]. The gravitational constant is not a force or acceleration but is employed as a scaling factor in Newton's Law of Gravitation, as demonstrated in **Error! Reference source not found. Error! Reference source not found.Error! Reference source not found.**[33][34].

$$F = \frac{Gm_1m_2}{r^2} \quad (1)$$

Equation 1. Gravitational Force Equation

Where:
F = gravitational force
m_1 = mass 1
m_2 = angle between the inclined plane and the base
r = distance between masses
G = universal constant ($6.67384 * 10^{-11}$ $\frac{\mathrm{m}^3}{\frac{\mathrm{s}^2}{\mathrm{kg}}}$)

Zero gravity ($0G$) describes a condition where there is an absence of gravitational force exerted on an object, which occurs either due to its infinite distance from any other gravitational body or when the net sum of all forces acting upon it equals zero [35]. Microgravity (μG) pertains to a state in which the net gravitational force exerted on an object is minimal, typically within the range of 10^{-4} to $10^{-6}G$ [36]. Although the object remains influenced by gravitational forces, it undergoes continuous free fall [36]. This perpetual free fall occurs when the object falls at a constant velocity but does not contact a surface [36]. As a result, the difference between the initial and final velocities manifests as a constant acceleration (g) [36]. Partial gravity refers to a gravitational force that is diminished but not absent compared to Earth's

gravitational acceleration, such as on the Moon, where gravity is approximately $\frac{1}{6}G$, on Mars $\frac{3}{8}G$, and on Earth $1G$ [29]. On Earth, the simulation of partial gravity can be achieved through techniques such as centrifugation, parabolic flight, or modified rotation devices that generate acceleration less than $1g$ [37].

To investigate gravitational effects, cell culturing is regarded as the most efficacious method, with bioreactors serving as the optimal apparatus, given their ability to supply controlled nutrients and biomimetic stimuli for cellular growth [38]. A bioreactor is defined as a vessel in which a chemical process involving organisms or biochemically active substances derived from such organisms is conducted, or a system designed for cell cultivation, first developed in 1964 (refer to **Error! Reference source not found.**) [39].

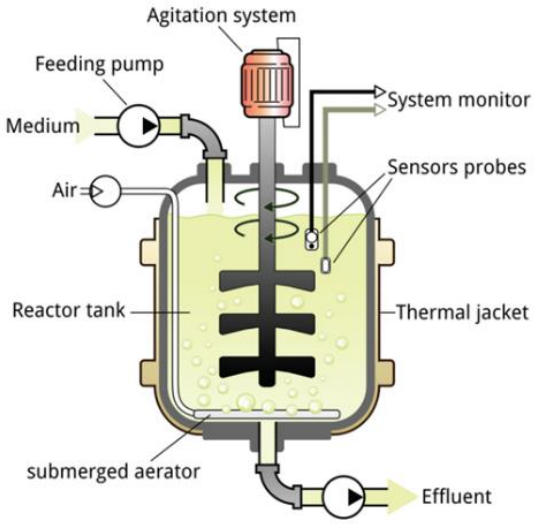

Figure 2. Basic Bioreactor
The figure shows the basic bioreactor components. It includes a feeding pump, air, medium, agitation system, reactor tank, and other elements to ensure an automated culturing system [39].

Previous bioreactors were designed as ground-based systems to mimic aspects of weightlessness or reduced gravity experienced by biological organisms in space. Recognizing this potential, in the mid-1980s, NASA researchers at the Johnson Space Center needed to develop a method to study the effects of microgravity on human tissues, as the shuttle fleet was grounded following the Challenger disaster [40]. They invented a rotating bioreactor to address the challenge of treating injured astronauts in space and to simulate weightlessness on Earth [40]. In μG, the bioreactor enables cells to grow in three-dimensional tissue structures that closely resemble natural development, facilitating advances in medicine both on Earth and in space [40]. In 2002, Houston-based Regenetech Inc. licensed NASA bioreactor technology and patents that can expand adult stem cells (from blood to bone marrow) by 50-200 times in less than a week, providing safer, faster, and more affordable cell sources for therapies [40].

Partial gravity bioreactors, although not extensively studied, have been previously examined. Research dating back to the 1900s has investigated the effects of clinostats, or rotating wall vessels, on biological samples [41]. Clinostats were invented by Julius Sachs, who rotated growing plants around their growth

axis [41]. These devices exist in one-dimensional (1-D) or two-dimensional (2-D) forms, depending on the dimensions of the rotated axial line or the entire experimental area [42]. Subsequently, enhancements to the clinostat with two axes led to the development of three-dimensional (3-D) clinostats, known as the Random Positioning Machine (RPM) (refer to **Error! Reference source not found.**) [42][43].

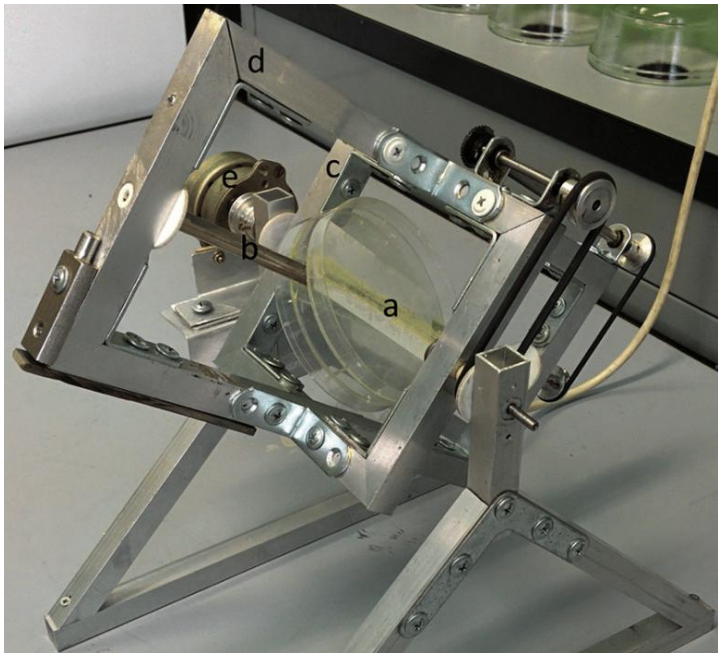

Figure 3. 3D Clinostat

The figure depicts a three-dimensional clinostat employed to investigate the effects of microgravity on seed germination: a, insert for Petri dishes; b, rotating shaft; c, inner frame; d, outer rotating frame; e, motor [43].

Numerous early-stage partial gravity bioreactors have been investigated using plant species capable of continuous growth under Earth's gravitational forces [44]. Initial implementations included clinostats, which maintain a constant rotation of a sample to effectively average the gravitational vector to near zero [41]. This form of a partial gravity bioreactor does not fully replicate “true” microgravity, as cells continue to experience mechanical stimulation and gradients that differ from actual microgravity conditions [41]. Subsequently, rotating wall vessel (RWV) bioreactors were introduced as a specialized variant of clinostats [41]. RWVs are fluid-filled cylinders containing cells, designed to create a low-shear, controlled environment conducive to cellular differentiation in three-dimensional space [45]. By rotating at a terminal velocity, RWVs facilitate the proper delivery of nutrients to the tissue culture, thereby promoting healthy tissue and cell growth [45]. In 2018, a previous senior design team utilized the stability of RWVs for cell culturing while incorporating the partial gravity factor using an inclined plane to partially cancel the gravitational vector, allowing cells to experience a form of partial gravity (refer to **Error! Reference source not found.**).

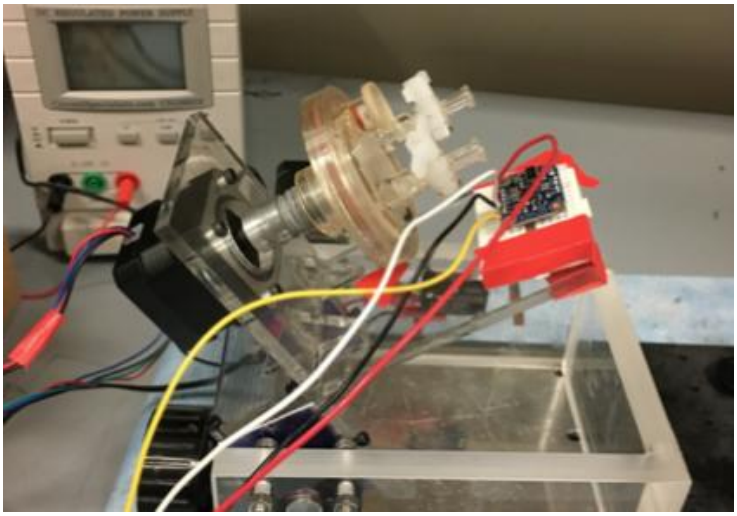

Figure 4. Partial Gravity Bioreactor
The figure depicts the prototype of a partial gravity bioreactor, designed by an earlier senior design team. It comprises a Rotating Wall Vessel (RWV) affixed to an inclined plane that simulates partial gravity.

1.3 Needs Statement

Building a partial gravity cell culturing prototype would enable the study of the relationship between cell properties and different gravitational environments, therefore allowing for correlation between gravitational differences and cell properties.

1.4 Implications of Project Success

In the event of the prototype's success, both terrestrial and extraterrestrial life would benefit significantly. Comprehending the effects of varying gravitational conditions on cellular behavior would facilitate more precise conclusions regarding human space exploration. Such findings would underpin the development of solutions aimed at safeguarding human safety beyond Earth. Facilitating human travel to outer space, including destinations such as Mars and the Moon, enhances our knowledge of extraterrestrial regions and addresses fundamental questions concerning alien life forms. Additionally, this research has the potential to identify new planets or locations in space where humans might establish a new life.

The success of the prototype closely correlates with several United Nations Sustainable Development Goals (UNSDGs) [46]. SDG 3: Good Health and Well-being is supported, as the device facilitates controlled studies on how partial gravity influences cellular development, physiology, and long-term health in space [47]. By understanding these effects, the prototype can inform the design of countermeasures, treatments, and potentially therapeutic approaches for conditions such as bone loss and muscle atrophy, which are of critical concern for astronauts [28]. Accordingly, the prototype would contribute to ensuring healthy lives for humans [47]. Furthermore, the prototype advances SDG 12: Responsible Consumption and Production by implementing a closed-loop biological system, an approach essential for sustainable

space habitats and beneficial for the efficient utilization of resources on Earth [48]. The use of a bioreactor enhances system control in cultivating cells, enabling accurate, real-time monitoring, early problem detection, reproducibility, and cost efficiency [49]. In this context, SDG 13: Climate Action is addressed by demonstrating how biological systems adapt to extreme and changing environments, thereby informing strategies for ecosystems on Earth [50]. Lastly, SDG 9: Industry, Innovation, and Infrastructure is pertinent, as the development of the prototype signifies an innovative research platform that represents the convergence of biotechnology and space technology [51].

2. Design Criteria

To guarantee the feasibility of the prototype, the design criteria are classified as either non-negotiable (mandatory) (refer to Table 1) or negotiable (desirable) (refer to Table 2). However, owing to the complexity of the project, these criteria are divided into two primary domains: partial gravity and the prototype.

2.1 Non-Negotiable Criteria

Four criteria must be satisfied to deem the partial gravity component in the project successful: gravitational type, simulation, visual validation, and movement.

Gravitational Type: With NASA deorbiting the ISS, the ability to conduct experiments in the unique microgravity laboratories would be impossible [52]. Therefore, gravitational experiments conducted on Earth should encompass the primary missions previously planned. According to NASA, traveling to the lunar surface and around the Moon would facilitate scientific discoveries that prepare humans for subsequent exploration, including Mars [53]. As the Moon and Earth represent the two most significant gravitational environments, lunar gravity ($\frac{1}{6}G$) and Martian gravity ($\frac{3}{8}G$) warrant careful consideration [54]. To obtain more accurate data, Earth's gravity ($1G$) and microgravity (μG) should also be included to ensure that the same cells are subjected to all gravity levels and to serve as references for previous experiments [54][55].

Movement: To cultivate cells effectively, the partial gravity method should not present any issues for cell culture practices. Given the high sensitivity of cells to their environment, the technique employed to simulate partial gravity must prevent excessive vibrations or inconsistent cell motion [56]. To accomplish this, the procedure for attaining different gravitational levels should function smoothly, enabling cells to undergo free fall while simultaneously minimizing shear stress on the cells and maintaining these conditions continuously.

Simulation: The partial gravity effect on cells has not yet been observed or tested. However, visualizing gravity is not applicable, since gravity is a theory [57]. Utilizing mathematics, fluid mechanics, and particle mechanics, a mathematical model should be developed for partial gravity.

Validation: Since models are simplified representations of the systems studied, models, to a degree, are all incorrect at least in some details [58]. Therefore, visualizing the specimen would provide further insight into the accuracy of the model and constitutes a form of validation. It is necessary to visualize the specimen under different gravitational levels to ensure the model's accuracy.

Five criteria should be met to consider the prototype successful: size, electrical safety, emergency safety, material, and specimen culturing stability.

Size: Since the prototype's placement may be limited to the incubator, its overall dimensions are also constrained. The Nuaire NU-5810E incubator is considered the most suitable and effective location based on previous designs because it operates at 37°C with 98% humidity [59]. The maximum size of the prototype is limited by the incubator's internal capacity, which measures $21 \times 17 \times 14\ in.$

Electrical Safety: For electrical safety, the standards established by the International Electrotechnical Commission (IEC), specifically IEC 60204-1, which outlines the general requirements for electrical equipment of machines (related to the safety of machinery), will be followed [60]. According to 'Safety of Machinery - Electrical Equipment of Machines - Part 1: General Requirements', a protective bonding circuit is required, ensuring all exposed metallic parts of the machinery are bonded and connected to a reliable ground [60]. This includes electrical enclosures and wiring, which should be organized neatly, clearly labeled, and protected, with cables rated appropriately for the voltage and current they carry [60]. Complying with EN 61010-2-030, Measuring Circuits and Test Equipment Safety Test, ensures the standard is met [61]. Since this is a prototype, comprehensive documentation—including electrical schematics, wiring diagrams, component lists, and user manuals—is essential.

Emergency Safety: As the prototype involves mechanical motion, there exists a potential for malfunctions. Consequently, ensuring the safety of the machinery is imperative. The International Standard ISO 13850, titled "Emergency Stop Function, the Design Principles for the Emergency Stop Function on Machinery", stipulates that an emergency stop is mandated when the machine presents a risk, and its implementation would mitigate this risk, as applicable to the prototype [62]. To comply with this standard, the emergency stop function should be activated by a human-initiated signal that remains engaged until it is manually reset [62]. Additionally, no start command should be effective during the operations halted by the emergency stop initiation, which must likewise be reset through human intervention [62].

Material: Given the potential placement of the prototype within an incubator, the selected materials must withstand both room temperature and 37°C, as well as 98% humidity [59]. Furthermore, the prototype is anticipated to maintain stability for at least four months.

Stability of the Specimen Culturing Component: Considering that the prototype integrates the cell culturing component and motion system responsible for partial gravity simulation, it is imperative that the attachment of the cell culturing component to the prototype's framework is secure to ensure precise results, given the sensitivity of cells to their environment [56]. Throughout any movement induced by the partial gravity simulation, the cell culturing section must remain stable; that is, it should neither wobble nor detach.

Table 1. Non-Negotiable Needs

Priority	Requirement	Metric	Target Values/ Range or Pass/Fail	Justification
Non-negotiable	Gravitational Type	Partial Gravity and Controls	Range: μG to $1G$ Lunar gravity ($\frac{1}{6}G$) Martian gravity ($\frac{3}{8}G$) Earth's gravity ($1G$) Microgravity (μG) [54][55]	NASA's Goals [53]
Non-negotiable	Partial Gravity Movement Causes Steady Flow	Partial Gravity Accuracy	Pass/ Fail Using Model and Visuals	Inaccuracy of data due to cell sensitivity [56]
Non-negotiable	Simulation	Mathematical Model	Pass/ Fail	Accuracy and Validation
Non-negotiable	Validation	Visual	Pass/ Fail	Accuracy and Validation of Model [58]
Non-negotiable	Size	Dimensions	$21 \times 17 \times 14\ in$	Nuaire NU-5810E Incubator Restricted Area [59]
Non-negotiable	Electrical Safety	Safety	Pass/ Fail of EN61010-2-030 [61]	IEC 60204-1 [60]
Non-negotiable	Emergency Safety	Safety	Pass/ Fail: should be activated by a human-initiated signal that remains engaged until it is manually reset, and no start command should be effective during the operations halted by the emergency stop initiation [62]	ISO 13850 [62]
Non-negotiable	Material	Strength and Durability	Pass/ Fail to withstand room temperature and 37°C, along with 98% humidity [59]	Project Duration
Non-negotiable	Cell Culturing Component Stability	Stability	Pass/ Fail of component wobbling/detachment	Inaccuracy of data due to cell sensitivity [56]

The table outlines the nine non-negotiable criteria essential for validating the prototype. Regarding partial gravity, the requirements encompass gravitational type, simulation, partial gravity movement, and verification processes. Regarding the prototype, the criteria related to the base and partial gravity—such as size, material, emergency safety, electrical safety, and the stability of cell-culturing components—are considered fundamental. Additionally, the metric, target range, and justification for each criterion are systematically provided.

2.2 Negotiable Criteria

Regarding the negotiable criteria, four factors have the potential to enhance the prototype if they are duly implemented. Firstly, the integration of an automated imaging system for cellular analysis would enable users to comprehensively evaluate cell culture and gain deeper insights into cellular interactions across various temporal stages. Secondly, the advancement of mathematical models into computational simulations would facilitate a more detailed understanding of the fluid dynamics affecting the cells. Thirdly, incorporating a broader spectrum of gravitational conditions would allow for a more precise simulation of human body movements, from Earth to extraterrestrial environments. Lastly, cultivating the cells would ensure that the prototype is suitable for cell culturing, with a cell viability exceeding 80%, in accordance with ASTM F2739-19 [63][64].

Table 2. Negotiable Needs

Priority	Requirement	Metric	Target Values/ Range or Pass/Fail	Justification
Negotiable	Automated Imaging System	Data Tracking	> 30 FPS	To record the cell's activity during culturing
Negotiable	Computational Models	Modeling Accuracy	Pass/ Fail	To have a more sophisticated model for partial gravity
Negotiable	Broader Range of Gravitation	Partial Gravity and Controls	More than four partial gravities achieved	To include minimal gravitational changes during spaceflight
Negotiable	Cell Culturing	Validation	Cell Viability >80% [63]	ASTM F2739-19 [64]

The table outlines the four negotiable criteria for enhancing the prototype. These criteria encompass an automated imaging system, the development of computational models, an expanded gravitational environment, and cell culturing. The table supplies the metric, target range, and justification for each criterion.

3. Solutions

The project concentrates on validating partial gravity, which involves ensuring that the tested specimen experiences the intended gravitational force. Cell culturing methodologies will not be addressed. To eliminate any effects attributable to cell culturing, the same culturing component will be employed across all proposed solutions.

3.1 Bioreactor Solutions

Bioreactors are the predominant method used in cell cultivation due to their ability to sustain biologically active environments and regulate parameters such as pH, temperature, oxygen tension, media perfusion rate, as well as their capacity to apply external stimuli [65]. Various types of bioreactors exist, including wave motion, stirred-tank, and rotating-wall vessels (refer to Supplementary Table S1) [66]. Since cells are susceptible to mechanical stresses such as shear forces and microfluidic flow, which may result in cellular structural failure and reduced viability, the selection of a bioreactor should be based on its ability to exert minimal shear stress on the cells [67]. Cells cultured in microgravity and ground-based microgravity analogs are presented with a low-shear stress environment suitable for cell cultivation [68]. Rotating wall vessels (RWVs) are effective for small volumes (< 10 L) and can simulate microgravity with low turbulence and minimal impact [66].

Given the same bioreactor employed for cell cultivation, two potential choices of the RWV used are examined. The solutions are based solely on the RWV's bubble issue.

Solution R.A: Standard Bioreactor

RWVs have been observed extensively to provide continuous sedimentation of particles through a culture medium [69]. The rotation provided by the RWV is special since it induces minimal cellular shear and turbulence [69]. Figure 5 shows the side view of a rotating wall vessel [70].

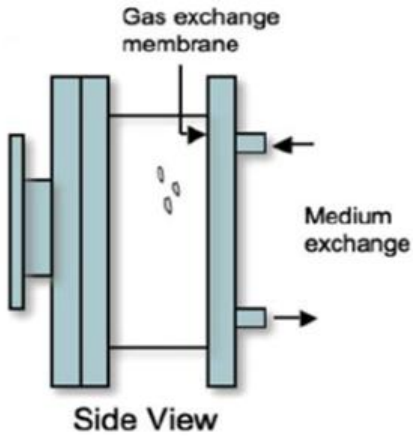

Figure 5. Schematic Side View of Rotating Wall Vessel Bioreactor

The rotation facilitates the complete immersion of the particle seeded in the medium. Consequently, using the standard RWV contributes to the advancement of knowledge in cell culturing. RWV systems have demonstrated success in cultivating prostate organoids, liver tissue, colon carcinoma, cartilage, and many other cell types [70].

Solution R.B: Bubble Trapping Bioreactor

One of the complications associated with RWVs is the formation of bubbles during operation [71]. The formation of bubbles interferes with the RWV environment, which includes zero headspace, low shear, and simulated microgravity [71]. Laminar flow needs to be developed so that the liquid within the bioreactor acts as a rotating object. A novel bubble capture HARV design would reduce and potentially eliminate the common issues of bubble formation while also reducing operational media volume without compromising the radius.

The bioreactor is designed with a hollow microporous plastic tube and an exit channel to catch bubbles. It is approximately 15 cm long to ensure proper perfusion through the microporous plastic (refer to Figure 6). The small, hollow tube, made of sponge-like plastic with tiny pores, has a plug placed partway down its length. When media is pushed down the tube, an exchange of old and new media occurs, providing nutrients to the circulating cells. This unique design enables the direct input of filling into the main bioreactor chamber, which is then output through a channel that captures bubbles and facilitates the exchange of used media (as shown in Figure 7) [72][73].

Although this design of bioreactor is more optimal, it can be successful only if the bioreactor is built and proven to not sustain any significant issues during construction within the short time for this project. Many small mistakes in the design of this system could compromise the fragile environment required to develop an RWV and cell culture environment [72][73].

Furthermore, bubbles or flow disruptions do not simply represent mechanical inefficiencies; they directly impact the ability of cells to remain in suspension, receive nutrients, and oxygen delivery. The presence of bubbles can also increase the shear forces affecting the cells.

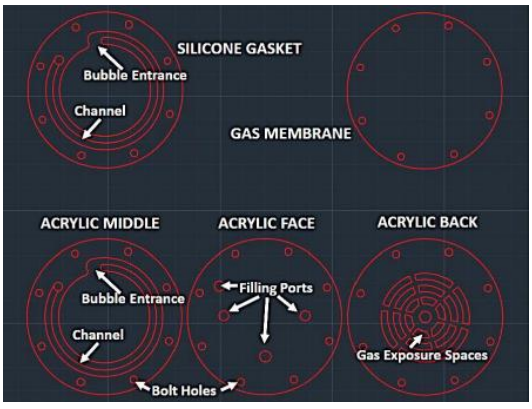

Figure 6. Design of Bioreactor

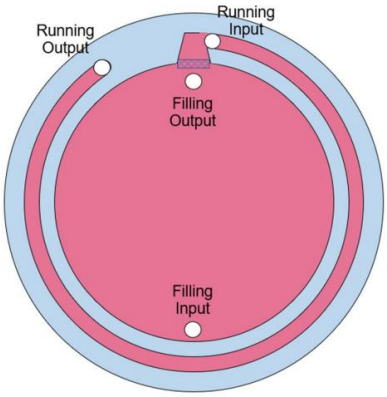

Figure 7. Bubble Trapping Bioreactor Sketch

3.2 Partial Gravity Solutions

Regarding partial gravity, three potential solutions for addressing this issue are examined.

Solution P.A: Inclined Plane (Dual Motors)

The proposed solution entails the enhancement of an existing design through the development of the partial gravity prototype using an RWV on an inclined plane, equipped with a dual-motor system (refer to **Error! Reference source not found.**8). The use of the inclined plane was previously studied and found to be a successful simulation of lunar gravity [74]. The design consists of three components: a foundational structure, a component that securely holds the bioreactor along with the motor responsible for generating rotational force, and a final system designed to adjust the angle of the motor and bioreactor to simulate partial gravity.

The base will be constructed as a rectangular structure capable of supporting the bioreactor assembly with stability and durability. The main section of the RWV will include a motor attached to the bioreactor to enable rotation, and this assembly will be mounted to the system that adjusts the bioreactor's angle. Next, a camera will be mounted on the same part of the device to accurately simulate the bioreactor's angle and allow monitoring of the cells during their rotation within the RWV. For the final part, a secondary motor capable of adjusting to various angles will be used, and it will be attached to the bioreactor system. The secondary motor should be able to set angle variations at least at four different positions to mimic the following gravitational conditions: $1G, \frac{3}{8}G, \frac{1}{6}G$, and μG. The rough sketch of the proposed solution is seen in **Error! Reference source not found.** 9.

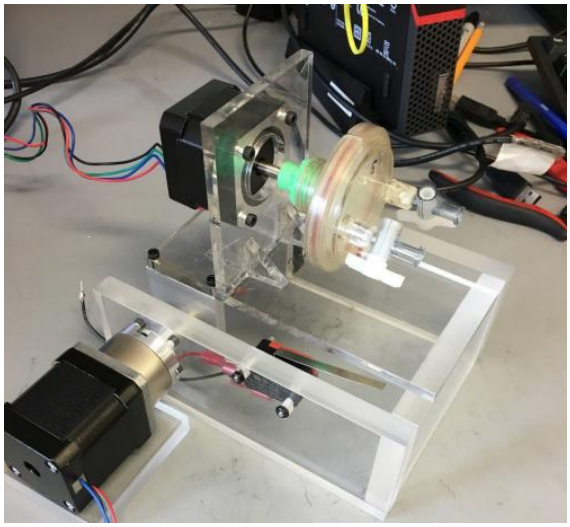

Figure 8. Inclined Plane Bioreactor with Dual Motors

The figure depicts the inclined plane bioreactor, designed by the previous senior design team. Utilizing two motors and an inclined plane, the previous team simulated partial gravity.

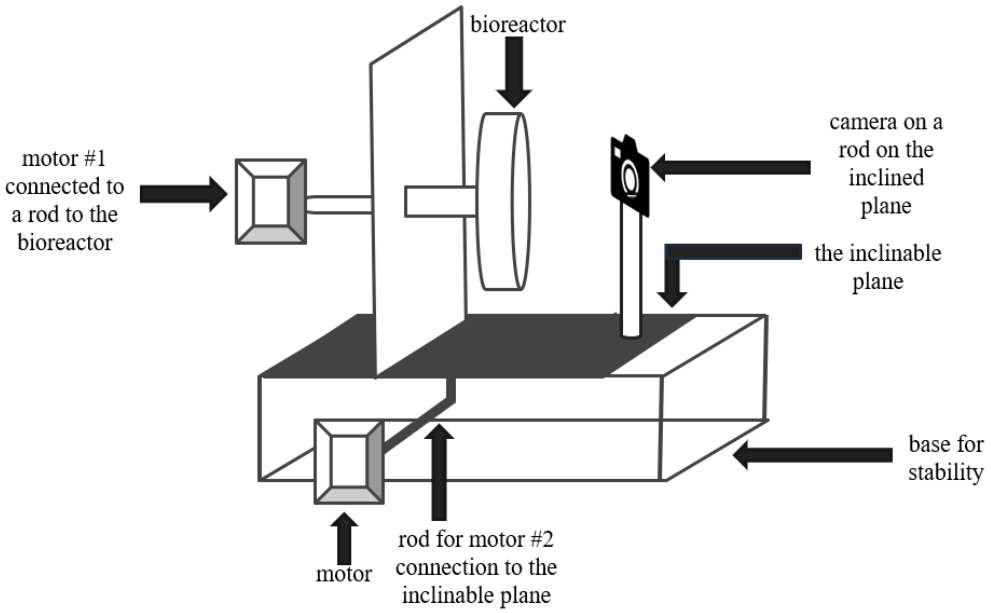

Figure 9. Rough Sketch of Inclined Plane with Dual Motors

The figure illustrates the preliminary sketch of the inclined plane setup with dual motors. The bioreactor is affixed to one motor, while the inclined plane is connected to another motor. The camera is positioned parallel to the bioreactor to ensure that the entire view of the bioreactor is captured.

These improvements to the current designs enhance the ability to validate the actual generation of partial gravities. The addition of a camera will enable real-time, accurate observation of cell reactions. Furthermore, this design provides a means for validation through modeling and mathematical analysis to confirm that this configuration produces the desired partial gravity effect for RWV.

Solution P.B: Four Centrifugations

The proposed solution concentrates on the centrifugation concept to emulate partial gravity on biological cells. The rationale for employing centrifugation is that the centrifugal force will generate an apparent gravity during rotational motion [75]. In fact, a proposed 0.16G acceleration was achieved by connecting two modules via a 300-meter tether and rotating them at 1 rpm [75]. O'Neill's 1.8 km radius Stanford torus, spinning at 1 rpm, produced Earth's gravity in space [75]. However, in numerous other examples and proposed solutions, the relationship between rotation and radius is closely interdependent. The centripetal acceleration is inversely related to tangential velocity when it remains constant, but has a direct relationship when angular velocity remains constant [76]. Consequently, centrifugation is a valid method for generating partial gravity, which can be as low as 0.001 G [77]. However, during centrifugation, it is crucial to rotate the system around its own axis to prevent sedimentation, as shown in Figure 10 [78].

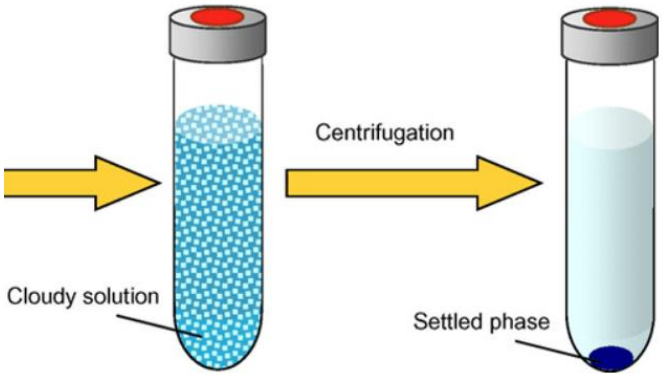

Figure 10. Schematic Diagram of Centrifugation to Settle Particles

The proposed solution emphasizes the capability to utilize a set of rotating bioreactors tailored for specific gravitational forces. As the system encompasses four distinct gravity levels, the solution entails four separate bioreactors, each stabilized by circumferential holes. These bioreactors would feature varying radii, enabling the simulation of partial gravity without subjecting the cells to undue shear stress from rotational motion and friction within the medium. Additionally, each bioreactor would be equipped with its own motor. Regarding the observational equipment, a camera will be positioned to provide a frontal view of all bioreactor surfaces, extending from the base of the prototype in an L-shaped configuration to encompass all units. Figure 11 illustrates the overall schematic of the design.

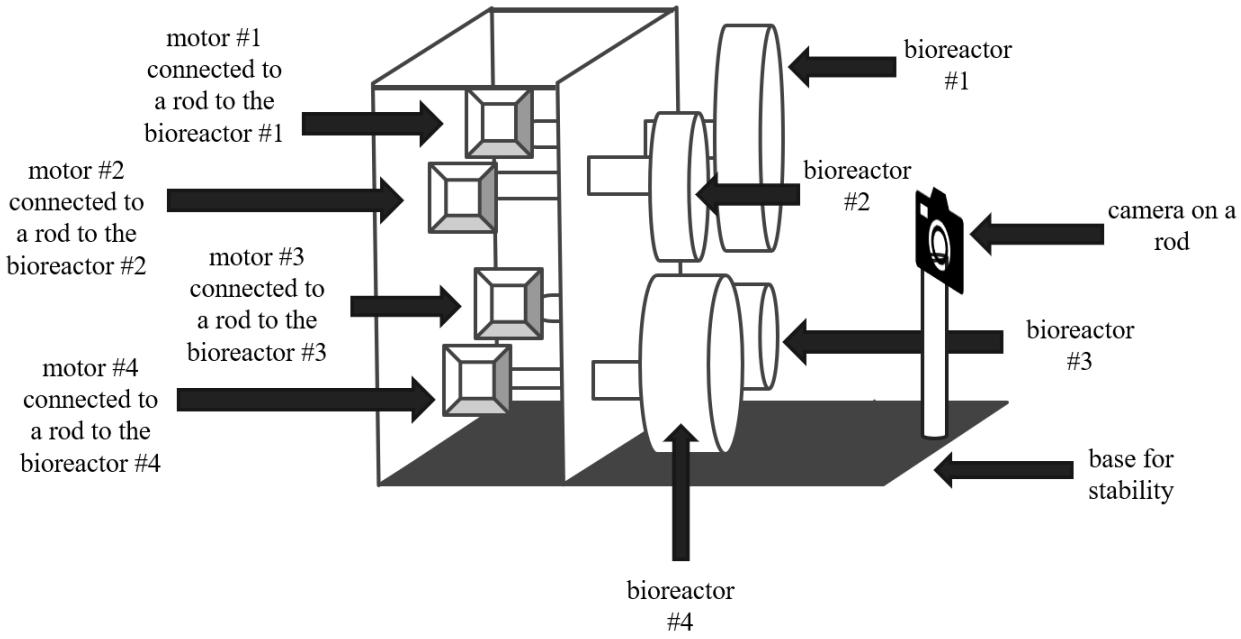

Figure 11. Rough Sketch of the Centrifugation Solution

There are four different bioreactors with different diameters, each attached to a motor. All the bioreactors are held in place by a vertical plane that has holes cut to the size of their diameters. The camera is placed to view the whole circumference of all the bioreactors.

Solution P.C: Inclined Plane (Single Motor)

This proposed solution outlines the use of an inclined plane single-motor bioreactor, equipped with an integrated camera monitoring system, as an innovative approach to enhancing the efficiency of cell culture processes. The system is engineered to optimize mixing, oxygen transfer, and gentle agitation—all vital for the proliferation of cells in suspension under partial gravity conditions. These hydrodynamic parameters can be quantitatively characterized using the specific power input (P/V), which correlates motor power with culture volume and serves as an essential metric to ensure proper mixing while preventing excessive shear forces. By maintaining P/V within the ranges established for mammalian and microbial culture systems, the design endeavors to balance nutrient and gas transfer requirements with the safeguarding of sensitive cell cultures [79].

For real-time visualization, the system will incorporate a camera with adjustable focus and LED illumination to ensure uniform brightfield imaging. To maintain consistent image quality during bioreactor operation, the camera shall be mounted directly onto the rotating vessel assembly, thereby following the vessel's motion and changes in orientation. This methodology guarantees that the camera sustains a constant field of view relative to the culture. The camera is affixed using a gimbal-like system, which permits the lens to remain aligned with the observation window throughout the entire range of vessel motion.

The control of the bioreactor is overseen by a microcontroller platform, such as Arduino, which regulates motor speed, acquires sensor data, and operates the camera. Data logging facilitates the export of sensor readings and image sequences for subsequent analysis. Safety features include overcurrent protection, temperature cutoffs, and emergency stop mechanisms to ensure the safety of both the vessel and its cultural contents.

The operation of rotation and tilt utilizing a single motor can effectively facilitate controlled vessel rotation; however, it demonstrates limited flexibility in adjusting the vessel's angle. In the simplest configuration, the motor drives the vessel at a fixed RPM, while the axis of rotation remains stationary; the angle relative to gravity is mechanically preset on the mounting frame. This configuration indicates that the speed and angle cannot be adjusted simultaneously, as the motor can execute only one function at a time. More sophisticated systems, such as differential gears, could be implemented; nonetheless, these systems introduce additional mechanical complexity, thereby reducing overall efficiency [79]. A rough sketch of the solution is seen in **Error! Reference source not found.**12.

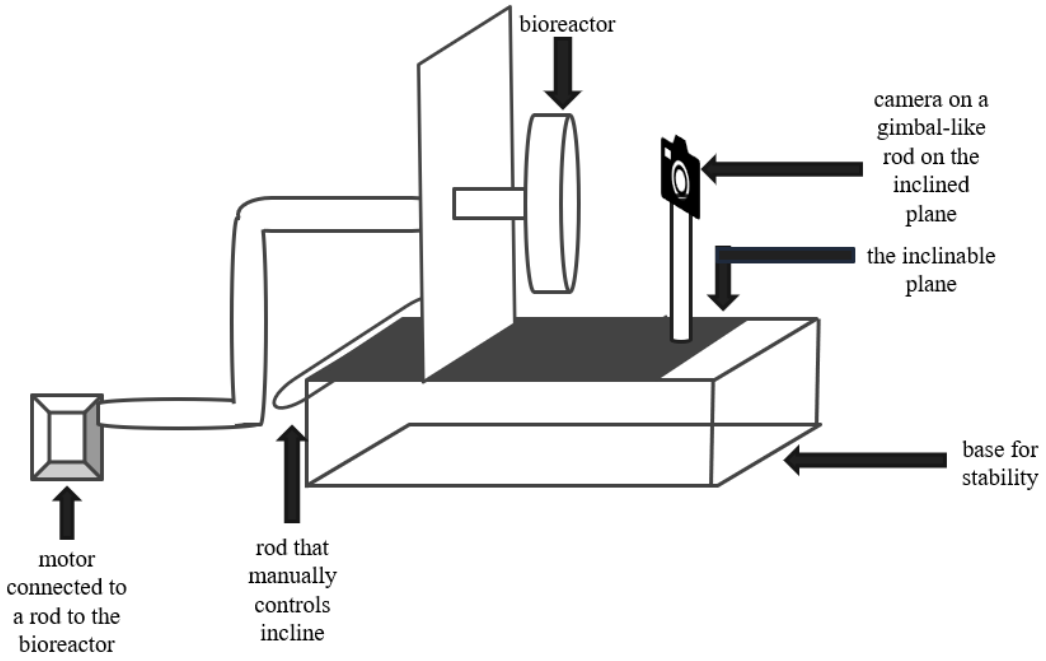

Figure 12. Rough Sketch of Inclined Plane with Single Motor

The figure illustrates the preliminary sketch for the single-motor inclined plane. The bioreactor is connected to the motor via a tube, and the incline plane is adjusted manually.

3.3 Decision Matrix

Selecting the appropriate approach for the bioreactor necessitates evaluating multiple factors, including availability, research utilization, and bubble formation. For the partial gravity scenario, the factors considered are design period, cost, feasibility, and cell viability. Given that each option possesses its own advantages and disadvantages, a weighted comparison is essential to identify the optimal solution. A prioritization (weighted decision) matrix is employed to evaluate the options based on predetermined criteria [80].

Regarding the bioreactor, the primary criterion to consider is availability. Since this prototype comprises two components, with a particular emphasis on the partial gravity section, the RWV is expected to have a minimal impact on the project timeline. Consequently, this criterion is assigned a score of 5 points. A score of 1 indicates that the component is either not accessible or requires design development. In contrast, a score of 2 signifies that it is accessible and does not necessitate any additional design efforts.

The second criterion pertains to research utilization: the number of literature papers that have employed the bioreactor. If research articles have utilized the bioreactor and data extraction occurred without issues, this suggests that the bioreactor is appropriate for use, or that its disadvantages do not outweigh its advantages. Given that the primary objective is to employ the bioreactor for research purposes, this criterion is assigned a weight of three points. A ranking of one indicates minimal usage in the literature, whereas a ranking of two signifies more widespread application.

Finally, the third criterion pertains to the formation of bubbles. Bubble formation represents one of the most limiting factors in data extraction and is therefore assigned a weight of three points. A rank of one indicates that bubble formation is present or disrupts fluid motion, whereas a rank of two signifies that bubble formation does not interfere with the flow of the medium. With these criteria established, the decision matrix is accordingly defined.

Regarding partial gravity, the initial criteria to be considered are the non-negotiable criteria. The primary criterion pertains to the gravitational type (refer to Table 1). Since the main objective is to attain $\frac{1}{6}G$, $\frac{3}{8}G$, $1G$, and μG to verify the locations' gravitational properties that NASA is reluctant to explore, the gravitational type criterion is assigned a weight of 5 points [54][55]. As this criterion requires simulations and theoretical applications, including fluid dynamics and other disciplines, the ranking is based on whether such gravitational values have been tested in previous experiments or through direct mathematical computations. A rank of 1 indicates minimal or no citations, whereas a rank of 3 signifies a higher citation count. The ranking process is conducted for each of the gravitational targets.

The second criterion concerns simulation (see Table 1). In relation to gravity, validation is based on mathematical principles and their effect on an object, considering that gravity is a theoretical framework [57]. The essential criterion states that the method's partial simulation of gravity should not increase shear forces nor disrupt fluid flow, which cannot be validated without simulation. Therefore, the mathematical simulation criterion is assigned 4 points. The ranking of this criterion is determined by its complexity, with 1 indicating the highest complexity and 3 the lowest.

The third criterion is visual validation (refer to Table 1). To confirm that the mathematical simulation accurately represents the system, the visual validation is assigned a weight of 3. The ranking of this criterion depends on the quality of specimen visualization, with 1 indicating difficulty in visualizing the specimen and 3 indicating clear visualization.

The fourth criterion relates to dimensions (refer to Table 1). When the device is situated within the incubator, its size is limited by the dimensions of $21 \times 17 \times 14\ in.$ Nonetheless, due to the design's substantial dependence on the type of bioreactor used and considering the restrictions related to dimension ranking, a score of two points is assigned. Consequently, this criterion is assessed based on the likelihood of space utilization, with a ranking of one indicating considerable spatial occupation and a ranking of three indicating minimal space consumption.

The final criterion relates to the project timeline. Considering that the project must be completed within three months, the proposed solution must adhere to this schedule. However, due to the dependency of the materials used in the device on procurement schedules and the arrival of supplies, this criterion shall be assigned a weight of 2 points. The ranking for this criterion is based on the ease of project replication, with a score of 1 indicating a prolonged or unprecedented process, and a score of 3 representing a swift completion. Once the criteria are established, the decision matrix is accordingly identified.

After evaluating the criteria for the bioreactor, as presented in Table 3, the standard bioreactor obtained the highest score of 19 points. Consequently, the selected bioreactor is the standard model. Upon assessing the criteria for partial gravity, as shown in Table 4, the inclined plane with dual motors achieved the highest score of 37 points, while the other solutions each scored 32 points. Therefore, the preferred solution is the standard RWV on an inclined plane with dual motors.

Table 3. Design Matrix for RWV Solutions

Criteria	Weight	Standard RWV		Novel RWV	
		Rating	Weighted Score	Rating	Weighted Score
Availability	5	2	10	1	5
Research Usage	3	2	6	1	3
Bubble Formation Disrupts Flow	3	1	3	2	6
Total Score			19		14

The table displays the criteria and their corresponding weights, which determine the favorable RWV solution. The rating and weighted score for each solution are shown. The standard RWV scored the highest.

Table 4. Design Matrix for Partial Gravity Solutions

Criteria	Weight	Inclined Plane with Dual Motor		Four Centrifugations		Inclined Plane with One Motor	
		Rating	Weighted Score	Rating	Weighted Score	Rating	Weighted Score
Gravitational Type	5	2	10	3	15	2	10
Mathematical Simulation	4	2	8	1	4	2	8
Visual Validation	3	3	9	3	9	2	6
Dimensions	2	2	4	1	2	2	4
Design Time	2	3	6	1	2	2	4
Total Score			37		32		32

The table shows the criteria and their weights, which determine the favorable partial gravity solution. The rating and weighted score for each solution are displayed. The inclined plane with dual motors scored the highest.

4. Engineering Design

The engineering design of the solution is founded upon detailed methodologies, calculations, and components to facilitate the successful execution of the partial gravity exerted on the cells. This section elucidates the calculations, mechanical plan, electronics, materials, and validation strategies employed to confirm that the selected options align with the system requirements.

4.1 Design Rationale

According to the most essential non-negotiable criteria, the prototype should have the ability to induce at least four different gravitational types: $1G, \frac{3}{8}G, \frac{1}{6}G$, and μG [54][55]. To simulate partial gravity on Earth, various methods, such as parabolic flight, centrifugation, or modified rotation devices, could be used [37].

The parabolic flight methodology allows researchers to conduct experiments under conditions of microgravity and partial gravity, thus simulating lunar or Martian environments in accordance with NASA's mission objective to facilitate human space exploration [81]. The technique utilized to recreate these conditions involves controlled maneuvers that temporarily induce free fall through the following procedures: pull-up, wherein the aircraft ascends at a steep angle (45º) enabling passengers to experience 1.8G; push-over, whereby, upon reaching the apex of the parabolic arc, the pilot reduces engine thrust, causing all objects inside the aircraft to descend together; reduced gravity, which occurs during the descent when no force acts upon the occupants, creating weightless conditions similar to those in space; and pull-out, where increased engine thrust and leveling out return the aircraft to Earth's gravity [81]. However, this approach has several limitations, including the short duration of reduced gravity, approximately 20 seconds per parabola, with typical flights comprising between 15 and 30 parabolas [81].

Centrifugation is employed to modify the magnitude of Earth's gravitational force in accordance with Einstein's Equivalence Principle, demonstrating that there exists no physical distinction between acceleration due to mass and linear acceleration [82, 83]. Operating a centrifuge at a constant velocity enables the sample to continually alter its direction and remain centered within the rotation [82]. Recognizing that the inertia of the sample and the rotation of the centrifuge collectively generate gravitational effects, the magnitude of this simulated gravity is dependent on the radius of the centrifuge and its angular velocity [82]. Centrifuges are utilized to mimic microgravity conditions through the Reduced Gravity Paradigm (RGP), which emphasizes the responses elicited by the difference between two levels of acceleration. RGP is most effective when applied to a stable and steady system operating at a high gravitational level before reducing the acceleration. Optimal results are observed in systems that respond rapidly; intermediate and slow responding systems require more extended periods than the available time interval to achieve the desired gravity level.

Given the significance of stability in centrifugation, modified rotational devices, including bioreactors, are assessed for their efficacy in partial gravity simulation. Bioreactors are biomechanically active systems engineered to replicate biological conditions by utilizing mechanical means to influence cellular processes through the meticulous regulation of biochemical and physical signals [84]. RWV, which employs vessel

rotation to generate low-shear mixing and simulated microgravity within the chamber, is available in two variants: the slow-turning lateral vessel (STLV) and the high aspect ratio vessel (HARV), as illustrated in Figure 13 [82]. The differences between these two types include the fact that STLVs incorporate a central cylinder oxygenator and can accommodate larger volumes. In contrast, HARVs are equipped with a gas-permeable member on one of their walls to enhance oxygenation [86][87][88].

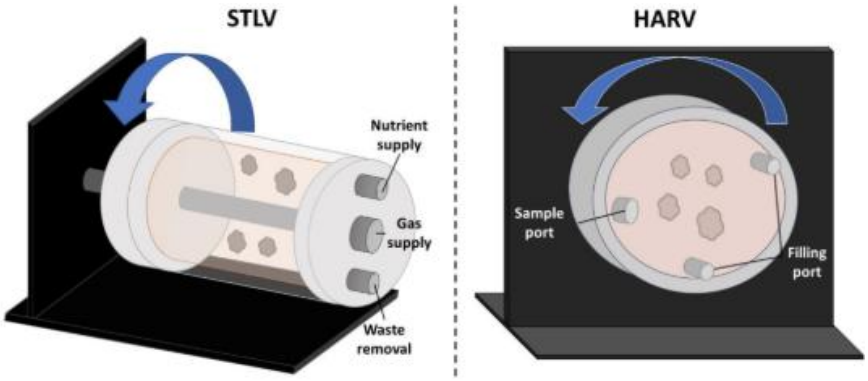

Figure 13. STLV vs HARV
The figure on the left depicts the STLV bioreactor, with its ports clearly labeled. To the right, the HARV is displayed, also with labeled ports. A cylindrical shape characterizes the STLV, whereas the HARV has a disc-shaped configuration [85].

Despite the limitations associated with the RWV, which include the requirement for high user competency, bubble formation, and the difficulty in determining the appropriate rotational speed to balance solid-body rotation with continuous freefall, the device enhances cellular performance through its capacity to improve mixing in low-shear environments substantially, facilitate high-density cell cultures and self-aggregation, promote cellular differentiation, and, notably, simulate microgravity. The effects of this simulation are well documented, encompassing alterations in calcium handling within cardiac cells and interference with cellular differentiation pathways [89][90][91].

The proposed solution emphasizes the integration of various benefits associated with different types of partial gravity simulation, while maintaining minimal adverse effects. To optimize cell growth, it is essential to cultivate cells in a manner that simulates free-fall. Consequently, maintaining a constant and steady rotation of the cells is necessary to ensure continuous exposure to free-fall conditions. This objective can be achieved by modifying the rotation of the RWV through the integration of centrifugation methods. As depicted in Figure 14, the device's orbit will be controlled to ensure a low-shear environment with a balanced solid-body rotation and continuous free-fall conditions [92].

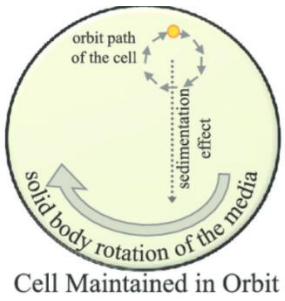

Figure 14. Orbit Trajectory of the Cell Within a Rotating Bioreactor

The orbital trajectory of the cell within a rotating bioreactor. The sustained rotation and sedimentation effects prevent the cells from settling at the base of the vessel. Additionally, the clockwise rotation of the medium facilitates the continuous suspension of cells in the orbit [92].

However, the centrifugation process would not accurately simulate the partial gravity of $\frac{1}{6}G$ and $\frac{3}{8}G$. With the inclination in the parabolic flight enabling a 1.8G simulation, the inclined plane within the solution would serve as the primary mechanism to achieve partial gravity conditions. In fact, NASA is presently constructing a Mars Artificial Gravity Habitat with Centrifugation (MAGICIAN) module to emulate Earth's gravity on Mars, as illustrated in Figure 15 [93].

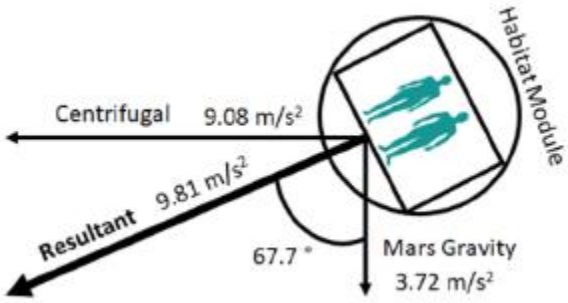

Figure 15. MAGAICIAN Schematic

A two-dimensional cross-section of the MAGIGAN modules displayed at an angle of 67.7° to achieve a resultant force equivalent to Earth's gravity [93].

Using a bioreactor would provide a controlled environment for cell growth, thereby reducing the likelihood of inaccurate data resulting from cell culture. Given that the bioreactor's rotation is maintained at a constant rate and the inclined plane's movement is solely a result of gravitational simulation, two motors will be employed. These motors will be identical to minimize potential complications in coding or wiring.

4.2 Calculations

To construct the prototype, specific calculations must be performed. These calculations will be utilized for simulation purposes to validate the prototype. To generalize the calculation, the specimen will be referred to as a particle; however, this term also applies to cells and the samples used during validation. Due to the numerous considerations involved in the calculation, the process will be divided into five sections: the inclined plane, sedimentation velocity, angular velocity, revolutions per minute, and cellular portion.

Incline Plane

The inclined plane facilitates the reduction of the gravitational force exerted on a particle by decomposing it into components. Referring to Figure 16, the gravitational force is entirely on one axis when $\theta° = 0° \; or \; 90°$ or decomposed into components. Utilizing trigonometry, Eq. 2 and Eq. 3 illustrate the values for the parallel and perpendicular components of gravity relative to the plane [94].

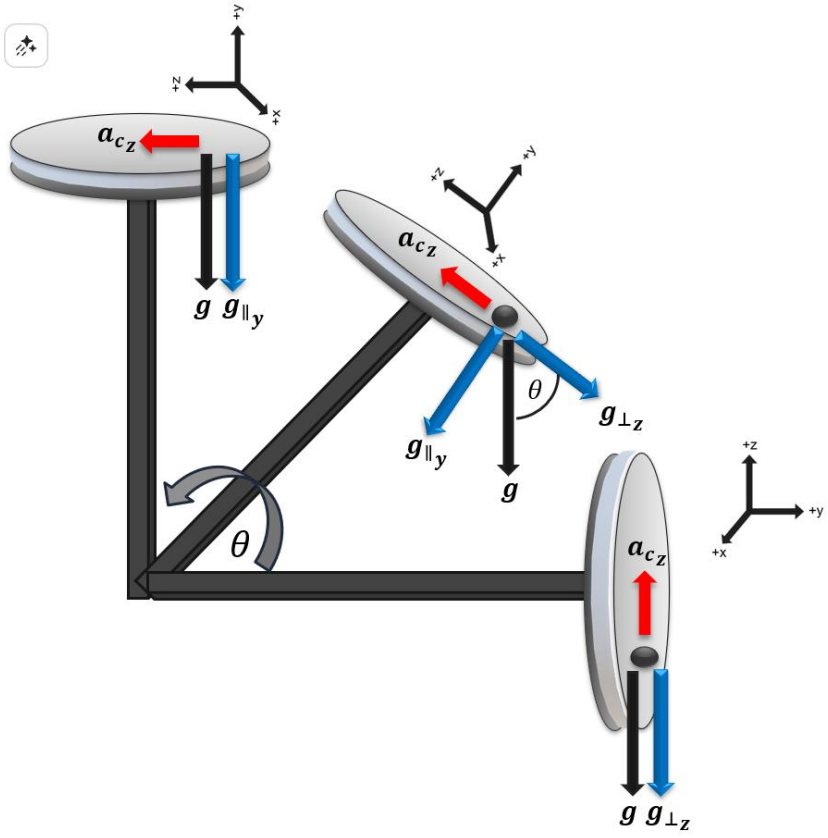

Figure 16. Free Body Diagram of a Bioreactor on an Inclined Plane

When the plane is parallel to the base, the gravitational force acts in the z-direction. When the plane is inclined at an angle θ from the base, the gravitational force is resolved into components. When the plane is perpendicular to the base, the gravitational force acts in the y-direction. The blue arrows represent the components of the gravity present in each scenario.

$$g_{\parallel_y} = g \sin\theta° \quad (2)$$

Equation 2. Parallel Gravitational Component

Where:
$g_{\parallel_y}$= gravitational component parallel to the plane
g = Earth's gravity ($9.81 \frac{m}{s^2}$)
$\theta°$ = angle between the inclined plane and the base

$$g_{\perp_z} = g \cos\theta° \quad (3)$$

Equation 3. Perpendicular Gravitational Component (Tangential Gravity)

Where:
$g_{\perp_z}$ = gravitational component perpendicular to the plane
g = Earth's gravity ($9.81 \frac{m}{s^2}$)
$\theta°$ = angle between the inclined plane and the base

Since the bioreactor remains stable along the y-axis, meaning it does not slide on the inclined plane, $g_{\parallel_y}$ is the effective gravitational force due to this stability, seen in Eq. 4. This is because the centripetal acceleration lies in the yz-plane, meaning the bioreactor rotates around the y-axis. Regarding, it is aligned with the axis of centripetal acceleration, making $g_{\perp_z}$ the gravitational component that balances the rotational acceleration. Therefore, solving Eq. 2 for in terms of θ, Eq. 5 shows the angle of the inclined plane that produces the effective gravitational force.

$$g_{tar} = g_{\parallel_y}$$
$$g_{tar} = g \sin\theta° \quad (4)$$

Equation 4. Targeted Gravity Case 1

Where:
g_{tar} = intended partial gravity
$g_{\parallel_y}$= gravitational component parallel to the plane
g = Earth's gravity ($9.81 \frac{m}{s^2}$)
$\theta°$ = angle between the inclined plane and the base

$$\theta = \sin^{-1}(\frac{g_{\parallel_y}}{g}) \quad (5)$$

Equation 5. Inclined Plane Angle

Where:
g_{tar} = intended partial gravity
$g_{\parallel_y}$ = gravitational component parallel to the plane
g = Earth's gravity ($9.81\frac{m}{s^2}$)
$\theta°$ = angle between the inclined plane and the base

Although the inclination angle equation establishes the environment in which the particle experiences modified gravitational forces, the particles should be in a state of "free fall" at any inclination position. Therefore, calculating the centripetal acceleration is necessary.

Centripetal Acceleration

Given that uniform and steady circular motion is requisite for laminar flow, centripetal acceleration will be employed. The centripetal acceleration (a_c) is directed towards the center, with the sole opposing acceleration being $g_{\perp_z}$. Therefore, the accelerations should be counteracting to ensure that no net force is exerted on the particle, as demonstrated in Eq. 6, with Eq. 3 and the substitution of the relevant quantities for a_c.

$$a_c = g_{\perp_z} \Longrightarrow$$
$$\omega^2 R = g\cos\theta° \quad (6)$$

Equation 6. Net Horizontal Acceleration

Where:
a_c = centripetal acceleration
$g_{\perp_z}$ = gravitational component perpendicular to the plane
ω = angular velocity
g = Earth's gravity ($9.81\frac{m}{s^2}$)
$\theta°$ = angle between the inclined plane and the base
R = radius of rotation of the particle to the center

The preceding steps are predicated on the initial assumption that the component of gravity parallel to the plane constitutes the target of partial gravity, as seen in Eq. 4, with the perpendicular component aligned along the same axis as the centripetal acceleration, thereby facilitating cancellation. Nonetheless, during circular motion, the particle does not remain fixed at a single position; instead, it encounters varying net accelerations at different locations. Consequently, two additional positions are calculated to delineate the RPM range necessary. Previously, it was assumed that the particle was only experiencing motion in one axis, as illustrated earlier in Figure 16. For the positions of interest, it shows another assumption that all accelerations exerted on the particle will partially cancel each other out until the desired net acceleration is achieved. This total acceleration is denoted as g_{tar}, where it stands for the intended partial gravity.

Eq. 7 shows the total gravity calculated from the free-body diagrams when the particle is at the top and the bottom.

$$g_{tar} = \sqrt{(\omega^2 R \pm g_{\perp_z})^2 + {g_{\parallel_y}}^2} \tag{7}$$

Equation 7. Targeted Gravity in Top and Bottom Placement

Where:
ω = angular velocity
R = radius of bioreactor
g_{tar} = intended partial gravity
$g_{\parallel_y}$ = gravitational component parallel to the plane
$g_{\perp_z}$ = gravitational component perpendicular to the plane

As for the sides, the particle will have the same equation as shown in Eq. 8.

$$g_{tar} = \sqrt{(\omega^2 R)^2 + {g_{\perp_z}}^2 + {g_{\parallel_y}}^2} \tag{8}$$

Equation 8. Targeted Gravity in Sides Placement

Where:
ω = angular velocity
R = radius of bioreactor
g_{tar} = intended partial gravity
$g_{\parallel_y}$ = gravitational component parallel to the plane
$g_{\perp_z}$ = gravitational component perpendicular to the plane

Being less detailed on the vector location and using the cosine rule, the intended partial gravity can also be calculated as seen in Eq. 9. However, in this equation, the angling of the plane does not have an effect.

$$g_{tar} = \sqrt{(\omega^2 R)^2 + g^2 + 2 * g * \omega^2 R * \cos\alpha^\circ} \quad (9)$$

Equation 9. Targeted Gravity in Overall Placement

Where:
ω = angular velocity
R = radius of bioreactor
g_{tar} = intended partial gravity
g = Earth's gravity ($9.81 \frac{m}{s^2}$)
α = angle between the gravity vector and the centripetal acceleration vector

Using Eq. 6 and solving for the centripetal acceleration in Eqs . 6, 7, 8, and 9, the centripetal acceleration at different positions of the system is given in Eq. 10.

$$a_c = g\cos\theta^\circ$$
$$a_c = \sqrt{{g_{tar}}^2 - {g_{\parallel_y}}^2} \pm g_{\perp_z}$$
$$a_c = \sqrt{{g_{tar}}^2 - {g_{\parallel_y}}^2 - {g_{\perp_z}}^2}$$
$$a_c = -g * \cos\alpha^\circ \pm \sqrt{{g_{tar}}^2 - g^2 * \sin^2\alpha^\circ} \quad (10)$$

Equation 10. Centripetal Acceleration

Where:
a_c = centripetal acceleration
g = Earth's gravity ($9.81 \frac{m}{s^2}$)
θ° = angle between the inclined plane and the base
g_{tar} = intended partial gravity
$g_{\parallel_y}$ = gravitational component parallel to the plane
$g_{\perp_z}$ = gravitational component perpendicular to the plane
α = angle between the gravity vector and the centripetal acceleration vector

Following the establishment of the connection for a_c, ω can be subsequently calculated.

Angular Velocity

Following the manipulation of Eq. 6, Eq. 11 was employed to isolate the angular velocity.

$$\omega = \sqrt{\frac{a_c}{R}} \tag{11}$$

Equation 11. Angular Velocity

Where:
ω = angular velocity
a_c = centripetal acceleration
R = radius of rotation of the particle to the center

RPM

Utilizing Eq. 12, the relationship between RPM and angular velocity is demonstrated [95].

$$RPM = \frac{60\omega}{2\pi} \tag{12}$$

Equation 12. RPM

Where:
RPM = revolutions per minute
ω = angular velocity

Substituting Eq. 11 into Eq. 12, Eq. 13 shows the RPM for the bioreactor.

$$RPM = \frac{60}{2\pi}\sqrt{\frac{a_c}{R}} \tag{13}$$

Equation 13. Bioreactor RPM

Where:
RPM = revolutions per minute
a_c = centripetal acceleration
R = radius of rotation of the particle to the center

The rotation of the bioreactor could be subsequently calculated. However, one of the limiting factors in its rotation is the linear velocity induced by the fluid moving tangentially. Therefore, it is necessary to determine the linear velocity of the system.

Linear Velocity

The fluid within the bioreactor exhibits tangential movement concurrent with rotation. Eq. 14 illustrates the relationship between angular velocity and linear velocity [95].

$$v = \omega R \tag{14}$$

Equation 14. Linear Velocity in Terms of Angular Velocity

Where:
ω = angular velocity
v = linear velocity
R = radius of rotation of the particle to the center

By substituting Eq. 11 into Eq. 3, Eq. 15 illustrates the linear velocity of the bioreactor.

$$v_{\perp} = \sqrt{R * a_c} \tag{15}$$

Equation 15. Tangential Velocity

Where:
$v_{\perp}$ = tangential velocity
a_c = centripetal acceleration
R = radius of rotation of the particle to the center

Given that the fluid possesses a tangential velocity, the particles suspended within it exhibit a sedimentation velocity. To facilitate “free-fall" conditions for the particles, the sedimentation velocity must be computed.

Sedimentation Velocity

Sedimentation velocity refers to the terminal velocity of a particle within a quiescent fluid [95]. At this velocity, the particle experiences no acceleration, as its terminal velocity remains steady. Utilizing Stokes’s law, the upward drag force resisting the particle's descent must be equal to the downward gravitational force [96]. However, Stokes’s law is predicated upon three fundamental assumptions:

1) The particle is small and spherical.
2) The particle does not rotate within the fluid.
3) Reynold’s number is considerably less than 1.

Although cells are not perfectly spherical, Stokes' law provides an approximate estimation of the terminal velocity. For simplification purposes, the extraction of the equation would be visualized in a 2D system. Referring to Figure 17, the particle is suspended within the fluid; therefore, the net force exerted on the particle can be calculated as shown in Eq. 16.

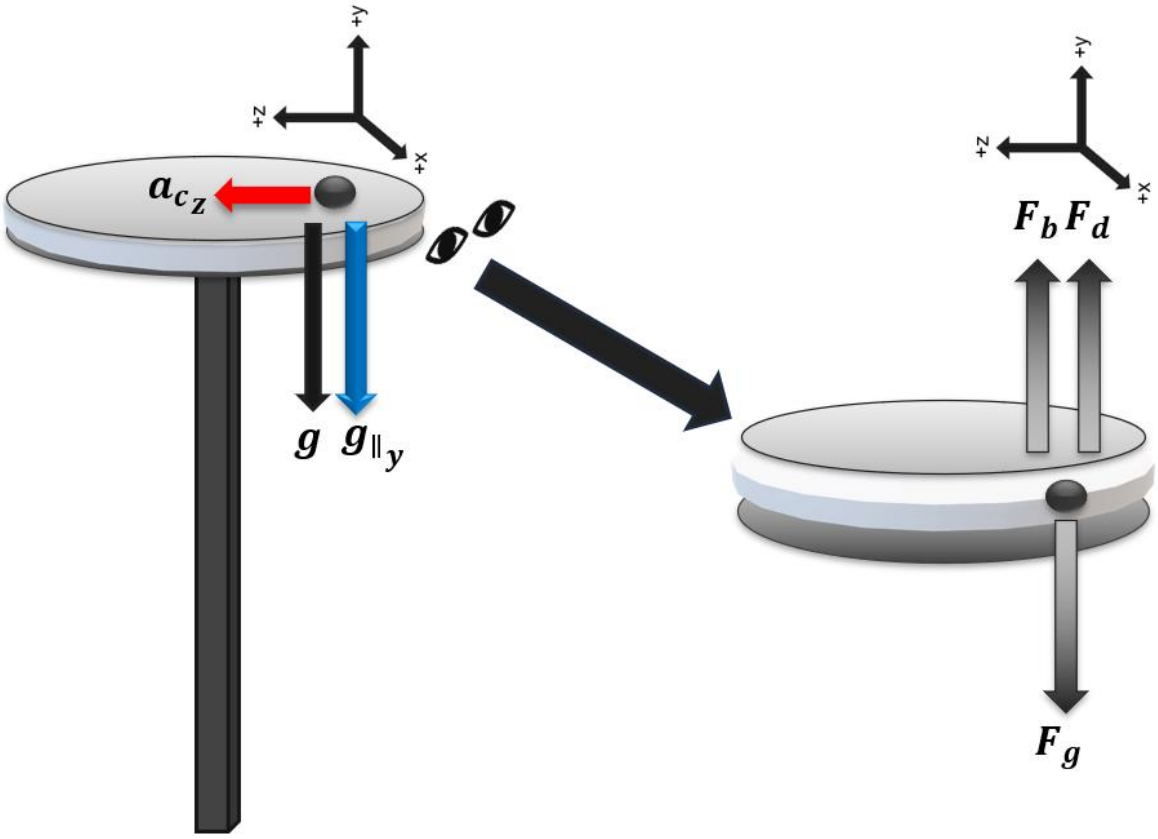

Figure 17. Free Body Diagram of the Particle in Fluid
The figure illustrates the forces acting upon the particle during its suspension within the fluid.

$$F_g = F_b + F_d \tag{16}$$

Equation 16. Net Driving Force on the Particle

Where:
F_g = gravitational force exerted on the particle (the gravitational component that causes the fall)
F_b = buoyancy force exerted on the particle
F_d = drag force exerted on the particle

Eq. 17 and Eq. 18 show the equivalence of the gravitational force (F_g) in a fluid and the buoyancy force (F_b), respectively [96].

$$F_g = V * \rho_p * g_{tar} \quad (17)$$

Equation 17: Equivalence of Gravitational Force

Where:
F_g = gravitational force exerted on the particle
V = volume of the particle
ρ_p = density of the particle
g_{tar} = intended partial gravity

$$F_b = V * \rho_f * g_{tar} \quad (18)$$

Equation 18: Equivalence of Buoyancy Force

Where:
F_g = gravitational force exerted on the particle
V = volume of the particle
ρ_f = density of the fluid
g_{tar} = intended partial gravity

Assuming that the particle's shape is spherical, the volume of the sphere is determined as shown in Eq. 19.

$$V_s = \frac{4}{3}\pi r^3 \quad (19)$$

Equation 19: Volume of Sphere

Where:
V_s = volume of the sphere
r = radius of the sphere

The drag force under consideration is that exerted on a spherical particle, as demonstrated in Eq. 20 [96].

$$F_d = 6\pi r \eta_f v_t \tag{20}$$

Equation 20: Drag Force

Where:
F_d = drag force exerted on the particle
r = radius of the particle
η_f = fluid viscosity
v_t = sedimentation velocity

Utilizing Eqs. 17-20, Eq. 21 is derived as the fully substituted form of Eq. 16.

$$\begin{gathered} F_g = F_b + F_d \implies \\ V_s * \rho_p * g_{tar} = V_s * \rho_f * g_{tar} + 6\pi r \eta_f v_t \implies \\ \frac{4}{3}\pi r^3 * \rho_p * g_{tar} = \frac{4}{3}\pi r^3 * \rho_f * g_{tar} + 6\pi r \eta_f v_t \end{gathered} \tag{21}$$

Equation 21: Fully Derived Net Driving Force on the Particle

Where:
r = radius of the particle
ρ_p = density of the particle
ρ_f = density of the fluid
g_{tar} = intended partial gravity
η_f = fluid viscosity
v_t = sedimentation velocity

The sedimentation velocity equation, as seen in Eq. 22, is derived from Eq. 21 [95].

$$v_t = \frac{2}{9*\eta_f}(\rho_p - \rho_f) * r^2 * g_{tar} \tag{22}$$

Equation 22: Sedimentation Velocity

Where:
v_t = sedimentation velocity
r = radius of the particle
ρ_p = density of the particle
g_{tar} = intended partial gravity
ρ_f = density of the fluid
η_f = fluid viscosity

Nevertheless, the values derived from the settling velocity are predicated upon various assumptions. To confirm that the particle remains in laminar flow, thereby validating the preceding calculations of sedimentation velocity, the Reynolds number (Re_p) should be computed [97]. The particle Reynolds number should be less than 2,000 to maintain laminar flow. If it exceeds 3,500, the flow becomes turbulent; for values in between, the flow is transitional [98]. By utilizing Eq. 23, these calculations can be confirmed [99].

$$Re_p = \frac{\rho_f * (v_p + v_f) * 2 * r}{\eta_f} < 2{,}000 \quad (23)$$

Equation 23. Particle Reynolds Number

Where:
Re_p = particle Reynolds number
ρ_f = density of the fluid
v_f = velocity of the fluid
v_p = velocity of the particle
r = radius of the particle
η_f = fluid viscosity

Given the presence of motion resulting in values of velocity, shear stress influences both the particle and the fluid. Shear stress is defined as the deformation of an object due to the application of a tangential force on its surface [100]. The maximum shear stress on the particle occurs at the circumference, as indicated by Eq. 24, which demonstrates the maximum shear stress on the particle [99].

$$\tau_{max} = \mu \frac{v_t * 3}{2 * r} \quad (24)$$

Equation 24. Particle Shear Stress

Where
v_t = sedimentation velocity
τ_{max} = maximum shear stress
μ = fluidic dynamic viscosity
r = radius of the particle

Regarding the fluid shear stress, it originates from laminar flow, resulting in varying fluid velocities at different levels [101]. Shear stress within the fluid can influence cellular integrity to such an extent that it may induce cell death [101]. Eq. 25 delineates the shear stress exerted by a Newtonian fluid on a surface [102]. This equation may be applicable in modeling the interaction between bubbles and particles [71].

$$\tau = \mu \frac{\partial v}{\partial r} \quad (25)$$

Equation 25. Fluid Shear Stress

Where
τ = fluid shear stress
μ = fluidic dynamic viscosity
$\frac{\partial v}{\partial r}$ = gradient of the fluidic velocity (shear rate)

Given that the fluid undergoes continuous rotation, the velocity gradient can be approximated by the tangential velocity of the system. Furthermore, since the initial simulation and calculations primarily focus on the maximum shear in all cases, the change in radius would not occur, implying that the radius remains the same. Accordingly, Eq. 25 can be expressed as shown in Eq. 26.

$$\tau = \mu * \omega R \quad (26)$$

Equation 26. Fluid Shear Stress

Where
τ = fluid shear stress
μ = fluidic dynamic viscosity
ω = angular velocity
R = radius of rotation of the particle to the center

With further comprehensive research, the shear stress could achieve higher accuracy. However, several experimental tests were conducted using a cylinder instead of a disc to measure the wall shear stress of specific fluids. Accordingly, the current values will be employed in the simulation until further updates are provided.

Dynamic Portion

To improve the mathematical model and obtain more precise RPM values, certain factors influenced by rotational effects must be considered. Cells undergo continuous growth during the culture process, which impacts the number of particles within the bioreactor. Consequently, the progression of cell growth over time is a critical factor. Although various models exist to describe cell growth, the exponential growth model will be employed to simulate the most extreme scenario, as described in Eq. 27 [103].

$$N(t) = N_o e^{rt} \quad (27)$$

Equation 27. Particle Growth Over Time

Where:
$N(t)$ = particle concentration over time
N_o = initial particle concentration
t = time (in hours)
r = population growth rate

Since particles act as barriers within fluids, increasing the particle quantity affects viscosity [104]. Using the model developed by Krieger and Dougherty, this impact on viscosity can be quantified. Eq. 28 shows the relevant equation for both low and high shear rates [104]. Assuming the particles are spherical, the maximum packing density is approximately 0.648, and the intrinsic viscosity is 2.5 [104].

$$\eta_{f,n} = \eta_f (1 - \frac{\phi}{\phi_{max}})^{-[\eta]*\phi_{max}} \quad (28)$$

Equation 28. Viscosity Change

Where:
$\eta_{f,n}$ = altered fluid viscosity
η_f = fluid viscosity initial (before adding particles)
ϕ = solid fraction in suspension
ϕ_{max} = maximum solid fraction in the suspension
$[\eta]$ = intrinsic viscosity that is dependent on particle shape

As the particle concentration increases, the solid fraction in suspension (ϕ) will change over time. Eq. 29 illustrates the variation of the solid fraction.

$$\phi(t) = \frac{N(t)*V_p}{V_f} \quad (29)$$

Equation 29. Dynamic Solid Fraction in Suspension

Where:
$\phi(t)$ = solid fraction in suspension (dynamic)
$N(t)$ = particle concentration over time
V_p = volume of one particle
V_f = volume of fluid

The viscosity change would then be dynamic, as seen in Eq. 30.

$$\eta_{f,n}(t) = \eta_f(1 - \frac{\phi(t)}{\phi_{max}})^{-[\eta]*\phi_{max}} \quad (30)$$

Equation 30. Dynamic Viscosity Change

Where:
$\eta_{f,n}$ = altered fluid viscosity
η_f = fluid viscosity initial (before adding particles)
$\phi(t)$ = solid fraction in suspension (dynamic)
ϕ_{max} = maximum solid fraction in the suspension
$[\eta]$ = intrinsic viscosity that is dependent on particle shape

Eq. 26 considers the fluid shear stress along with the dynamic viscosity. As shown in Eqs. 29 and 30, changes in particle concentration result in variations in fluid viscosity. Additionally, to maintain the system's integrity and prevent particle failure or death, the rotational velocity must be properly adjusted. Therefore, using Eqs. 26 and 30, Equation 31 depicts the dynamic fluid shear stress.

$$\tau(t) = \eta_{f,n}(t) * \omega(t)R \quad (31)$$

Equation 31. Dynamic Fluid Shear Stress

Where
$\tau(t)$ = fluid shear stress (dynamic)
$\eta_{f,n}(t)$ = altered fluid viscosity (dynamic)
$\omega(t)$ = angular velocity (dynamic)
R = radius of rotation of the particle to the center

With that, the RPM needs to be adjusted according to the changing conditions. Utilizing Eq. 12, and 31, the RPM change equation is seen in Eq. 32.

$$RPM(t) = \frac{60}{2\pi}(\frac{\tau(t)}{\eta_{f,n}(t)*R}) \quad (32)$$

Equation 32. Dynamic Bioreactor RPM

Where:
$RPM(t)$ = revolutions per minute (dynamic)
$\eta_{f,n}(t)$ = centripetal acceleration
R = radius of rotation of the particle to the center
$\tau(t)$ = fluid shear stress (dynamic)

4.3 Numerical Sampling

Numerical sampling shall be employed to validate the equations extracted in the Calculations section. However, before calculating theoretically, it is necessary to discuss the basis for the assumption to validate the results. RPM values from 0 rpm to 1300 rpm are expected [105]. An rpm of 1300 is anticipated to be extreme, with a maximum exposure duration of 10 minutes to cells before their death [105]. As for Re_p being 2,000, there is a high possibility of cells flowing in laminar flow, such as endothelial cells in blood flow [106][107].

Given that osteoblasts are the most frequently used cells for the validation of partial gravity in culture systems, the particle considered within the system would be an osteoblast cell [108][109]. As this represents first-order numerical sampling, cell-to-cell interactions have not yet been incorporated into the model. Consequently, it will be assumed that the cells do not interact with one another.

The osteoblasts possess a diameter ranging from 20 to 50 micrometers [110]. Considering that cellular water content varies between 60% and 80%, the cell density marginally exceeds that of water, which is estimated at approximately 1.050 $\frac{g}{cm^3}$ [111]. Since the cells are predominantly cultured in Dulbecco's Modified Eagle Medium (DMEM) supplemented with 5% fetal bovine serum (FBS), the density is 1.005 $\frac{g}{cm^3}$, and the viscosity is characterized as $0.862 mPa.s$ [112][113].

Consequently, numerical values could be determined. Given the presence of multiple variables, a code (refer to Supplementary Code S 1) was employed to obtain the results. As mentioned above, there were three different methods used to calculate the RPM and the angle needed to achieve the desired gravity. From the calculations, some imaginary values appeared in certain portions, indicating that it would not be realistic to attain the intended gravity in this specific location. Additionally, due to the balancing of the vectors, some positions resulted in high RPM values. However, to ensure that the particles (specifically the cells) are not harmed by the motion caused by rotation, we will use the lowest RPM and angle pair for each intended gravity, as shown in Table 5.

Table 5. Numerical Values of Initial RPM and Angle Values

Gravity ($\frac{m}{s^2}$)	Inclined Angle (°)	RPM ($\frac{rev}{min}$)
$1G$	90°	5
$\frac{3}{8}G$	86°	49.9
$\frac{1}{6}G$	88°	35.3
μG	0°	10

The table presents some of the final numerical values derived from the equations detailed in the Calculation section. The table includes four different values of gravity and their respective incline angles, along with the RPM corresponding to a specific bioreactor radius of 0.025m. Laminar flow was confirmed using Reynolds' number.

Correlation and Analysis

After calculating both the sedimentation velocity and the tangential velocity, the ratio of these velocities offers valuable insights into the interactions among the particles within the fluid. If the sedimentation velocity surpasses the tangential velocity, it indicates that the particles would settle, which is undesirable. Conversely, if the terminal velocity is lower than the tangential velocity, it suggests that the particles remain in suspension continuously. The objective is to ensure that the tangential velocity exceeds the terminal velocity. The correlation is

$$v_t > \approx v_\perp$$

If this condition is not satisfied, adjustments to the system should be implemented.

Figure 18 illustrates the correlation between the RPM and the radius. The correlation is

$$RPM \propto \frac{1}{\sqrt{R}}$$

, considering the centripetal acceleration is kept constant. Therefore, as the radius increases, the RPM decreases.

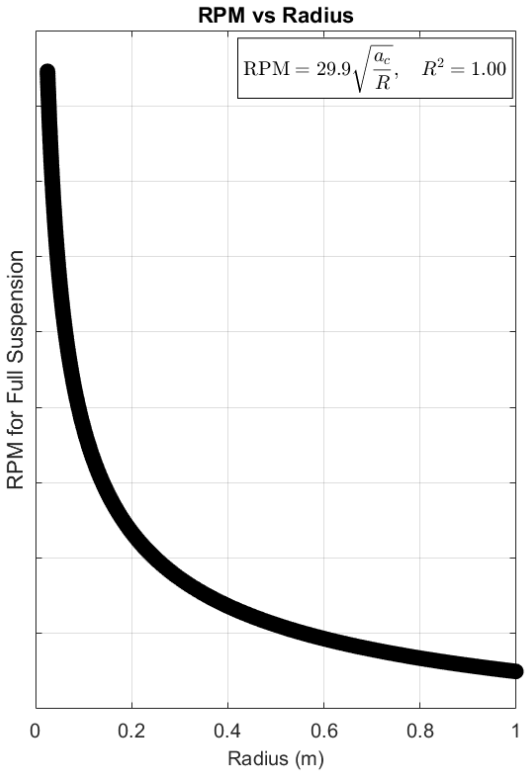

Figure 18. RPM vs Radius
The figure illustrates that increasing the bioreactor radius decreases RPM.

4.4 Simulation

Given the presence of a few mathematical equations, a simulation can be conducted.

Mathematical Simulation

The mathematical simulation relies on the equations presented in the Calculation section. The detailing of the simulation would be discussed more accurately in upcoming papers.

5. Components

After understanding roughly how the system works, the choice of the right components is essential.

5.1 Motor, Driver, and Microcontroller

Given that a maximum of 1300 rpm is considered extreme when sustained for more than 10 minutes, as exceeding this limit could result in cell denaturation, a smaller radius is preferable for maintaining healthy cell cultures [105]. Regarding view clearance, a significant aspect of the prototype involves visually assessing the particle during rotation and inclination. Therefore, the bioreactor chosen should have a small radius and a large view area. The camera has yet to be selected, depending on the bioreactor that will be utilized.

As for the motor, to find the intended torque, Eq. 33 is used by plugging in Eq. 5 to solve for a_c and Eq.12 to solve for ω.

$$\begin{gathered} \tau = m * R_b * a_c \implies \\ \tau = m * R_b * \omega^2 * R_b \implies \\ \tau = m * {R_b}^2 * (\frac{2\pi}{60} * RPM)^2 \end{gathered} \tag{33}$$

Equation 33. Torque

Where:
τ = torque
m = mass
R_b = radius of rotation of the particle to the center
RPM = revolution per minute

Having a safety factor of 2, the torque equation will be multiplied by 2. Eq. 34 shows the equation to get power.

$$P = \omega * \tau \implies \quad (34)$$
$$P = \frac{2\pi}{60} * RPM * \tau$$

Equation 34. Power

Where:
τ = torque
P = power
RPM = revolution per minute

The calculations shall be conducted based on the most adverse scenario. The maximum values for mass, radius, and RPM are 3.00 kg, 0.0495 m, and 313 rpm, respectively. The RPM value is roughly 10 times the maximum RPM that will be run in the system. Basing the motor on a significantly higher RPM would enable more experimental research to be conducted on the prototype. The mass was obtained from calculations performed by the previous senior design team. The torque and power computed using Eqs. 33 and 34 are 7.89 Nm and 259 W, respectively. The safety torque is 11.8 Nm, using a safety factor of 2.

A suitable motor option is the NEMA 34, 470 in.-oz stepper motor, which has the required torque and a 1.8° step angle [115]. The motor's maximum temperature is 120°F, exceeding the incubator's temperature [115]. Additionally, the motor has a maximum current per phase of 4.2A and operates at 48V DC [115]. Considering that this component is a stepper motor, a stepper driver has been selected to facilitate more precise rotational movement. The designated stepper driver is characterized by a current per phase ranging from 2.35A to 8A [116]. Its operating voltage spans from 24V DC to 75V DC, with a maximum temperature threshold of 185 °F [116]. These specifications make the driver compatible with the motor and suitable for deployment within the incubator. Furthermore, the maximum step resolution is one hundredth, allowing the driver to divide a complete step into 100 smaller steps [116]. This enhances the variation in increments between the angles in the prototype, thereby enabling a broader range of inclination solutions.

The microcontroller employed for direct motor control is the Arduino UNO Wi-Fi REV2, which incorporates the ATmega4809 microcontroller [117]. The 8-bit ATmega4809 microcontroller offers the highest flash memory capacity of 48 kB [117]. The input voltage range is from 6 to 10V, which is lower than that of the driver, rendering it suitable for the application [117]. Most notably, this Arduino features 14 digital input/output pins, facilitating a more direct and organized wiring system [117]. A key feature of this Arduino is its capability to connect to Wi-Fi. It is equipped with an ECC608 crypto chip accelerator that enables Wi-Fi connectivity [117]. Additionally, it possesses Bluetooth connectivity capabilities [117]. Unlike more advanced Arduino models, this Arduino can be controlled both wirelessly and via physical connections, functioning similarly to the Arduino Uno Rev3 [117]. This dual functionality allows for the integration of both components within the prototype. Establishing a wireless connection is crucial to ensure that the controlled environment remains regulated, particularly through the modulation of the incubator's opening and closing mechanisms.

5.2 Base Material

Acrylic sheets shall be utilized as the foundational material for the prototype [118]. Given that the prototype will be positioned within the incubator and the tests are anticipated to be conducted therein, the humidity and temperature within the incubator are likely to influence the base material of the prototype.

The physical properties of the acrylic sheets, as determined by the ASTM method D648, show that a thickness of 0.236mm has a deflection temperature under a load of 264 psi of 99 °C, and the forming temperature ranges from 170 to 190 °C [118]. The softening point, as determined by the ASTM method D1525, is 115 °C, with a maximum recommended continuous service temperature of 82 °C [118]. Since the incubator would have a temperature significantly lower than the temperatures stated above, the minimum width of the acrylic sheets would be 0.236mm.

Additionally, the electrical properties of the acrylic are those of a good insulator, with a surface resistivity higher than that of most plastics, making it a viable protector of the electrical components in the prototype.

Due to exposure to humidity, the acrylic is expected to expand by 0.6%, 0.4%, and 0.2% for humidities of 100%, 80%, and 60%, respectively [118]. This would be incorporated into the design limitations.

Additionally, we need to ensure that the prototype will not degrade in the presence of chemical additives. Another limitation is the use of isopropyl alcohol (the most used alcohol in labs). Acrylic has limited resistance to this chemical [118]. Therefore, it is advisable to avoid using alcohol on the surface or placing the prototype on a surface with alcohol to ensure longevity. However, since there is limited resistance, it will be stated that limiting the use of alcohol is a must.

5.3 Rod

To achieve the inclination angles, the plane must undergo rotation. This rotation is facilitated by connecting the inclined plane to a rod that transfers linear motion into rotational motion. The choice of material for the rod is critical for the viability and safety of the prototype. Accordingly, aluminum is selected as the material for the rod.

A primary characteristic of aluminum is its combination of lightness and strength [119]. Given that the inclined plane, in conjunction with another motor and the bioreactor, will contribute to the overall weight that the rod must support, aluminum presents as the most suitable material. Nonetheless, simulations must be conducted to determine the precise width necessary for the prototype. As the rod will be supported at its end, it is advantageous that the material's weight does not augment the stresses at these points.

Additionally, aluminum has a melting point of 660°C, which is higher than the temperature inside the incubator, ensuring its stability [119]. Regarding the incubator, aluminum is non-corrosive due to a protective oxide layer; however, it can corrode if exposed to highly alkaline or acidic environments for an

extended period [119]. Therefore, it is advisable to be cautious and avoid direct contact between aluminum and acidic or alkaline chemicals [119]. As a safety feature, aluminum is ductile and malleable [119]. In the event of failure, aluminum absorbs significant energy before breaking and deforms before failure [119]. This property provides a visual warning that the prototype may be at risk of failure before it happens.

5.4 Bioreactor

In contrast to the conventional bioreactor, the innovative bioreactor should be constructed utilizing the template derived from a prior design [71]. Given that the original CAD model was unavailable, assumptions regarding the diameters were formulated based on the data provided in the design methodologies. Furthermore, considering the bioreactor's specifications, the dimensions are deemed to remain valid [71]. The structural layers of the bioreactor are as follows: top plate, bubble plate, gasket, spatial area, gas membrane, and bottom plate.

Figure 19 illustrates the top plate, which contains the inlet, outlet, and bubble exit, each with a diameter of 4 inches. Figure 20 illustrates the bubble-capturing plate, with the blue spiral indicating the path of the bubbles. Following this layer, a silicon gasket is installed to prevent leakage within the bioreactor. The subsequent layer is characterized by its spatial arrangement, which facilitates the rotation of particles and fluid. The next layer comprises the gas membrane, enabling gas exchange between the particles inside the bioreactor and the external environment. Finally, Figure 21 presents the bottom plate, with the slits surrounding the center serving as the gas exchange interface. Since each layer is separated, all the layers have cut-out holes around their circumference. The layers are then stacked on top of one another and bolted together.

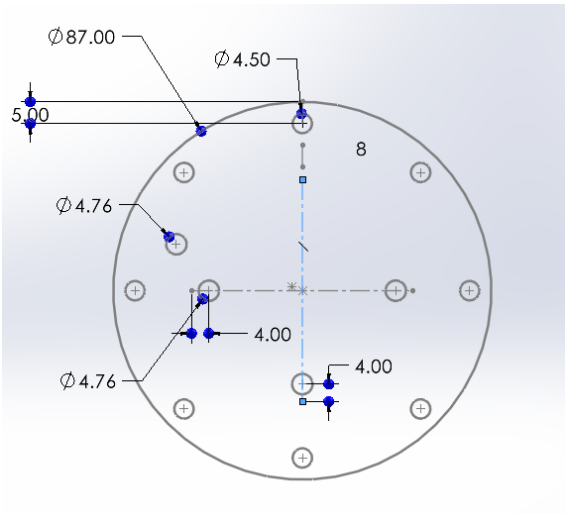

Figure 19. Top Plate of Bioreactor
All dimensions are in mm.

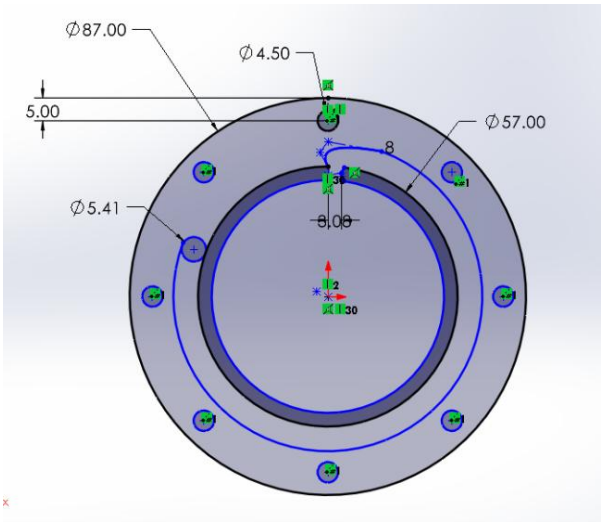

Figure 20. Bubble Capturing Plate of Bioreactor
All dimensions are in mm.

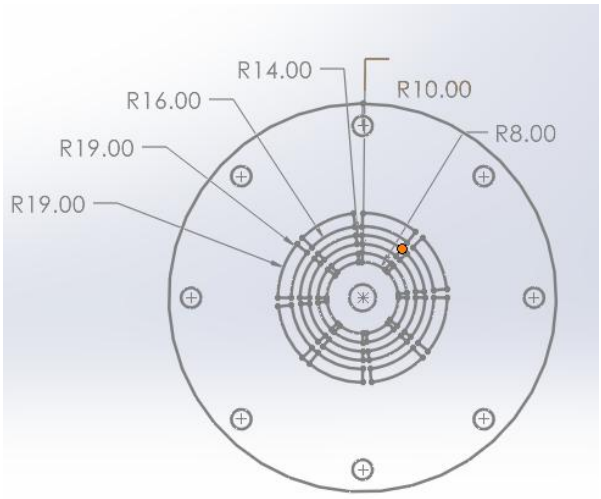

Figure 21. Bottom Plate of Bioreactor
All dimensions are in mm.

6. Prototype

6.1 Wiring

After discussing the components of the prototype, various electrical components will require connections. Initially, it is essential to possess two motors and two stepper motor drivers. The rationale for this requirement is that one motor will be connected to the bioreactor to facilitate its rotation, and the other motor will be attached to the rod that rotates the plane. Considering that the motors used have high torque, it is impractical to connect both to a single driver. Connecting them to a single driver would result in current division between the two motors. Since these motors demand more than three-fourths of the available current, such a setup would increase hazards and compromise system safety. Although procuring two drivers incurs higher costs, electrical safety remains a primary consideration in design. Additionally, this would allow the wiring to be neat, following the prototype's needs.

The motors have four wires, which should be connected to the corresponding terminals on the stepper motor driver: A-, A+, B-, and B+. The stepper driver is interfaced with the Arduino via the following connections: STEPS+, DIRECTION+, ENABLE+, and GND. The STEP+ connection regulates the number of steps, thereby controlling the rotation of the shaft. The DIRECTION+ connection determines the direction of rotation. The ENABLE+ connection specifies whether the rotational system will be operated manually or exclusively by the driver.

The negatives of STEP, DIRECTION, and ENABLE shall be connected to GND. While this is not obligatory, ensuring they remain disabled would enhance safety. Concerning GND, the entire system must be referenced to a common ground to provide safety and to comply with wiring standards.

Given that emergency safety is a critical requirement of the prototype, the activation of the stop button must result in the halt of all system motion. Accordingly, the VCD of the drivers is linked to one terminal of the stop button, while the opposite terminal is connected to the power source (power plug). The Arduino is powered independently via a battery, ensuring a dedicated power supply. Nevertheless, the battery grounds the Arduino, which is also connected to the GND of the drivers, thereby ensuring uniform grounding across all components. The block diagram illustrating this configuration is presented in Figure 22.

Using Fritzing, Figure 23 illustrates the electrical connections in the breadboard view, while Figure 24 displays the corresponding schematic.

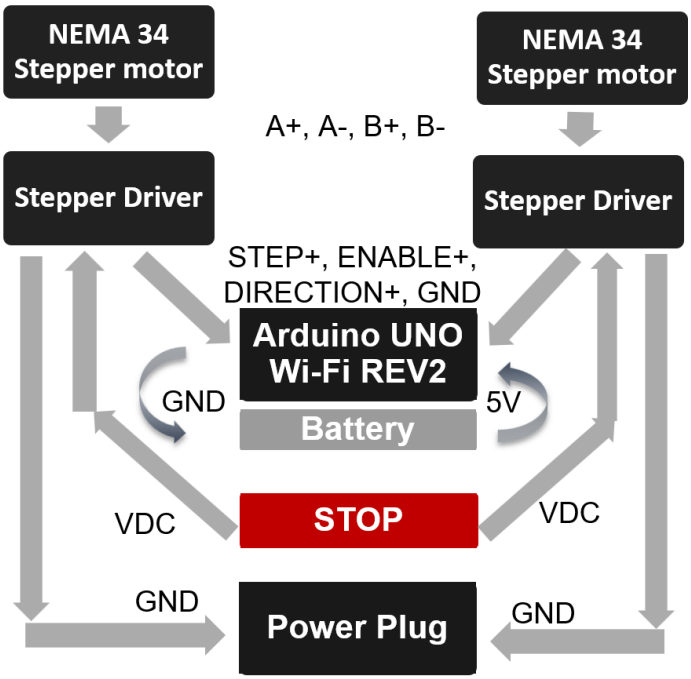

Figure 22. Flow Diagram of Electrical Connections

The figure shows the block diagram of the electrical connections in a simplified manner.

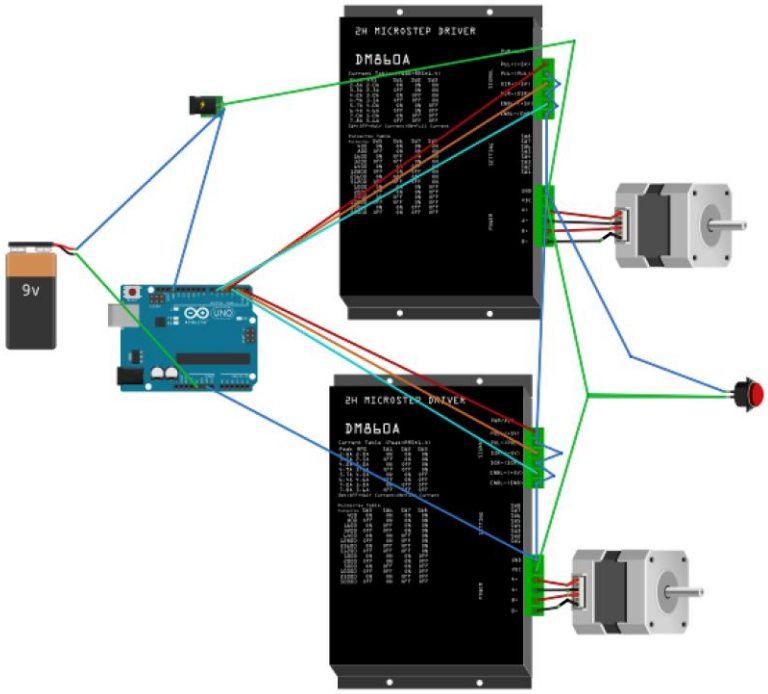

Figure 23. Breadboard View of Electrical Connections

The figure shows the connection of the two motors to two separate stepper drivers. The drivers are connected to the Arduino, which is connected to the battery. The drivers are also linked to an emergency button via their VDC and are grounded to the Arduino, which in turn is grounded to the battery.

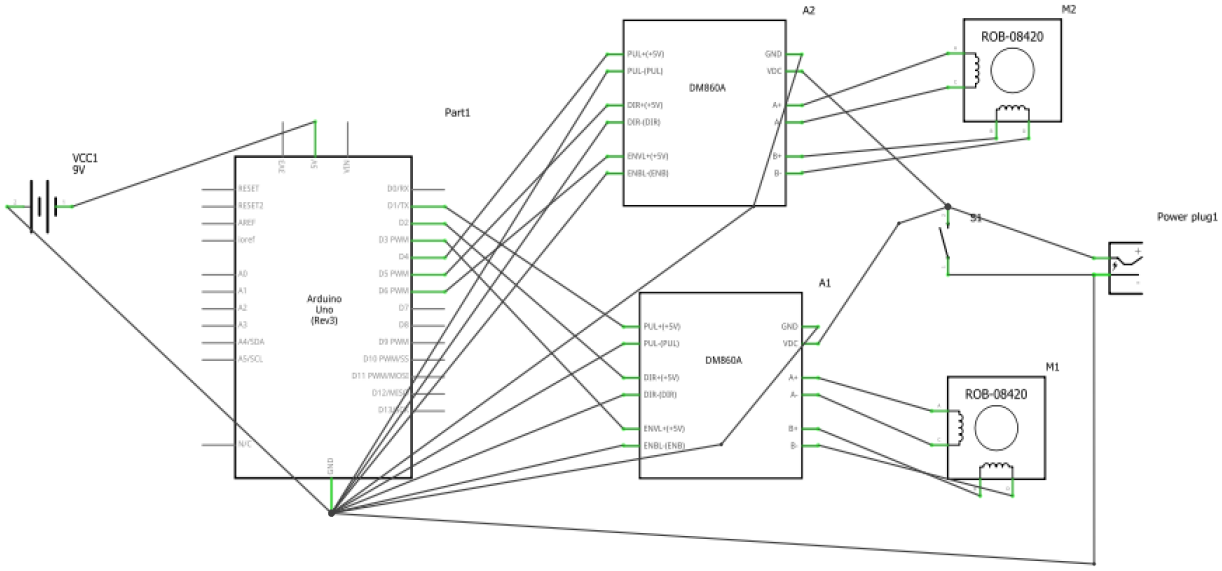

Figure 24. Electrical Connection Schematics

6.2 Overall Prototype Basics

With the components assembled and the electrical connections established, the prototype could then be constructed.

Constrained by the dimensions of the incubator, the prototype should not exceed the specified limits of the incubator: $21 \times 17 \times 14\ in$. As Figure 25 and Figure 26 illustrate, the dimensions of the initial prototype estimate are significantly smaller than these constraints, with a value of $11.9 \times 11.4 \times 2.95\ in$. The dimensions provided are not final; however, they represent the maximum allowable measurements for the prototype. The length has yet to be finalized due to the current inability to incorporate the final components, the bioreactor and camera.

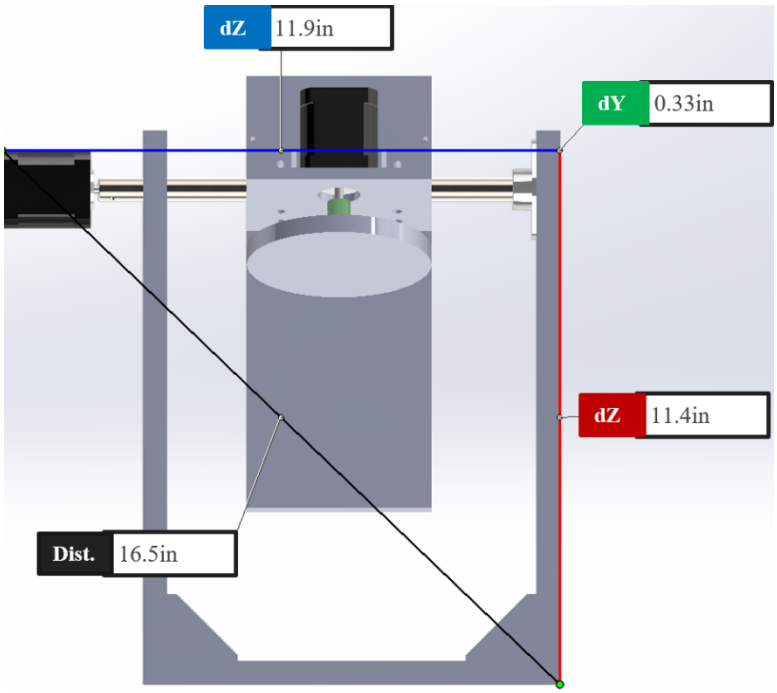

Figure 25. Top View with Dimensions

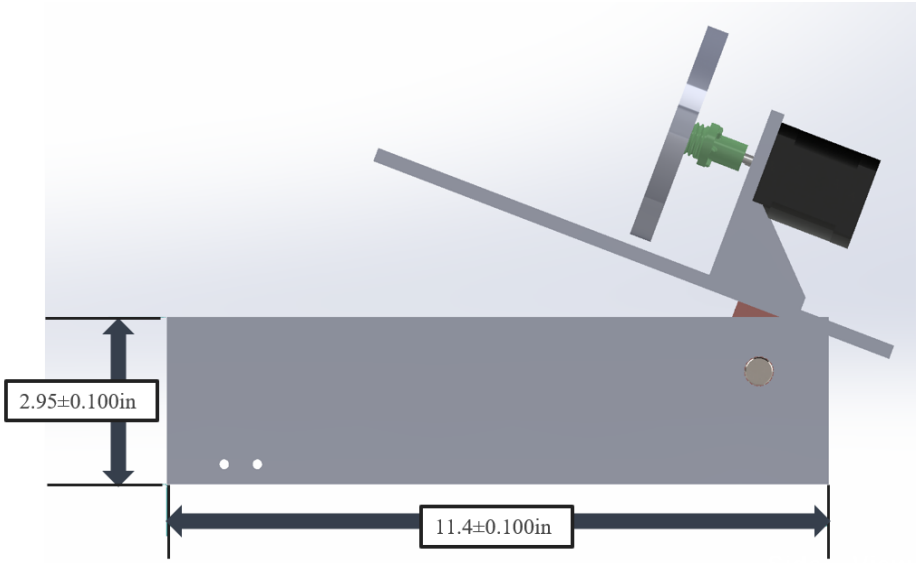

Figure 26. Left Side View with Dimensions

The prototype initially comprises a rectangular acrylic sheet base. An aluminum rod is positioned along two parallel sides of the base. The aluminum rod ensures that the inclined plane can rotate, as the movement of the inclined plane requires a certain angle. The most straightforward and effective method to facilitate this rotation automatically is by using a rotatable rod.

To enable the rotation of the rod, it must be connected to a suitable motor capable of facilitating such motion. Accordingly, the rod is affixed to the NEMA 34 stepper motor, as depicted in Figure 27. Since the diameter of the rod remains unspecified, it is presently connected directly to the motor shaft. This arrangement presumes that the aluminum rod possesses a screw hole to secure the motor shaft and that the diameter of this hole matches that of the motor shaft. Should this not be the case, a motor coupler would be utilized to establish the connection.

Nevertheless, it is imperative to secure the aluminum rod in position. To achieve this, bearings are installed at both ends of the rod. A ball bearing is positioned at the end nearer to the motor to facilitate smooth rotation and to prevent increasing stress on the motor shaft. The rod is subsequently connected to the inclined plane via two square brackets. These brackets fit snugly into the rod through their circular holes and are fastened to the inclined plane at the horizontal section. The horizontal section attached to the inclined plane supports the bioreactor and the motor. The bioreactor is coupled to the motor using the motor coupler illustrated in Figure 28. The motor is secured in place by being screwed to the horizontal section.

The base is secured using L-shaped brackets to ensure stability. Furthermore, the inclined plane and the bioreactor plane are also supported by L-shaped brackets. The additional components in the prototype include a modification to the thickness of the front width of the base to ensure that the inclined plane does not topple from the initial angle. A stop button will also be installed. The camera will be positioned at the end of the inclined plane. The method of attachment remains under consideration, as the camera has not yet been selected.

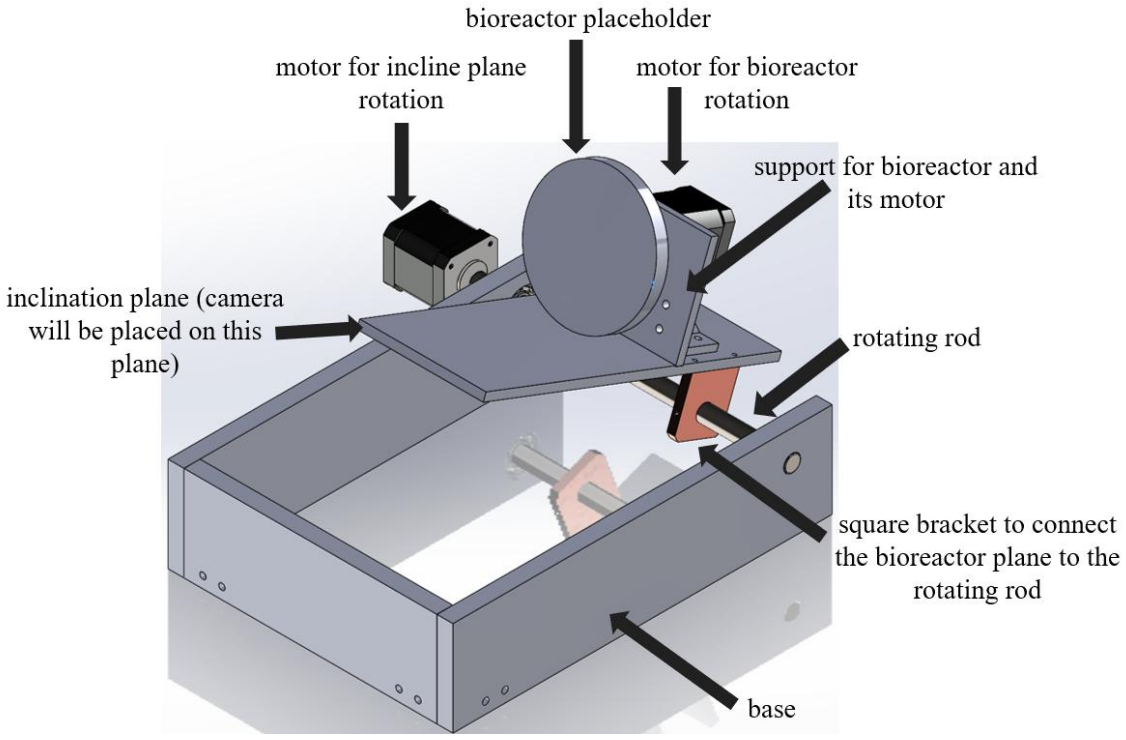

Figure 27. Top Right-Angled View of Prototype CAD

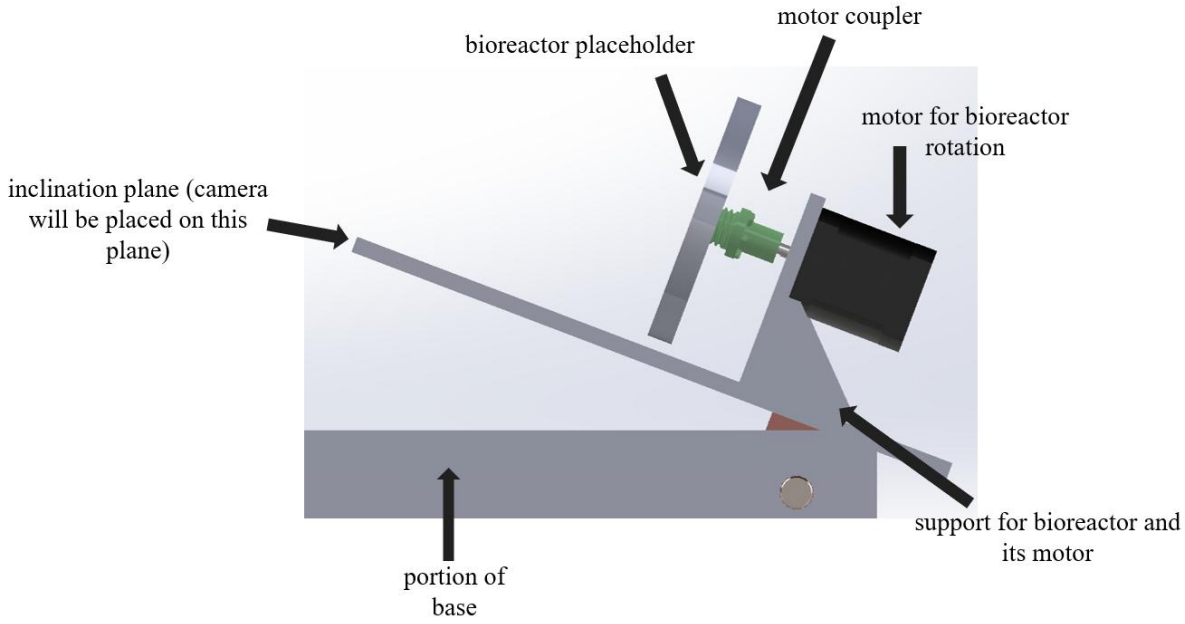

Figure 28. Left Side View of Prototype CAD

7. Test Method

To guarantee the validity of the results and decisions, specific tests must be conducted.

7.1 Visual Assessment Camera Placement

The visual validation primarily relies on positioning the camera clearly so that the interior of the bioreactor is visible. For this purpose, a protocol has been established.

Utilizing at least two distinct phone cameras, three photographs will be captured from each viewpoint, with the camera parallel to the circular side of the bioreactor, as assessed by the observer. Using a ruler, the distance between the camera and the bioreactor will be documented in an Excel file. For every bioreactor, at each viewpoint, a minimum of three photographs will be taken at three different magnifications. This methodology aims to provide a broader range of magnification options, considering that the camera has not yet been acquired. Each image will be imported into MATLAB, and photo analysis will be employed to identify the visible area. The area values will subsequently be analyzed in JMP using the Fit Model procedure to assess statistical significance. Ultimately, the largest statistically significant area will be used to determine the optimal camera distance and magnification.

A decision will be made after measuring the areas of the camera choices.

7.2 Validation of Fluid Dynamics Using Alginate Beads

To validate the partial-gravity bioreactor and fluid dynamics, alginate beads can be added to visualize the motion of particles. Developed from a calcium chloride solution, they have similar densities to that of a cell. Due to the increased size of alginate beads, the bioreactor would have to run at 15 rpm.

The alginate beads do not confirm the existence of a partial-gravity environment; however, they accurately represent the forces and fluid dynamics occurring within the novel bioreactor to verify that an appropriate environment is being created within the device. This validation will directly influence whether it is possible to culture cells within the bioreactor.

8. References

1) "April 1961 - First Human Entered Space - NASA," NASA. Available: https://www.nasa.gov/image-article/april-1961-first-human-entered-space/

2) "Croatian Barrel Theory," Google Books. Available: https://books.google.com/books?hl=en&lr=&id=6fpgEQAAQBAJ&oi=fnd&pg=PR3&dq=why+are+the+rings+around+the+planets+for&ots=6NYg8vGXx7&sig=fDnYWiJSO_0-C7OTs6DVDOnjzG8#v=onepage&q=why%20are%20the%20rings%20around%20the%20planets%20for&f=false

3) "Croatian Barrel Theory | Miro (Mike) Laus," Mike Laus. Available: https://www.miromikelaus.com/#:~:text=Grounded%20in%20Laus%E2%80%99s%20cultural%20heritage%2C%20the%20Croatian%20Barrel,system%2C%20with%20celestial%20bodies%20emerging%20at%20varying%20times.

4) A. May, "10 Wild Theories About the Universe," Live Science, Jul. 16, 2021. Available: https://www.livescience.com/strange-theories-about-the-universe.html

5) R. H. Sanders and S. S. McGaugh, "Modified Newtonian Dynamics as an Alternative to Dark Matter," Annual Review of Astronomy and Astrophysics, vol. 40, no. 1, pp. 263–317, Sep. 2002, doi: 10.1146/annurev.astro.40.060401.093923. Available: https://doi.org/10.1146/annurev.astro.40.060401.093923

6) B. Famaey and A. Durakovic, "Modified Newtonian Dynamics (MOND)," arXiv.org, Jan. 28, 2025. Available: https://arxiv.org/abs/2501.17006

7) NASA, "Studying Combustion and Fire Safety - NASA," NASA, Mar. 07, 2024. Available: https://www.nasa.gov/missions/station/iss-research/studying-combustion-and-fire-safety/

8) Gullari, Jeevan Kumar. (2025). The Impact of Moon Phases on Earth, Plants, and Humans: A Comprehensive Study from Project Alpha. 10.13140/RG.2.2.12235.71203. Available: https://papers.ssrn.com/sol3/papers.cfm?abstract_id=5090101

9) J. Green, D. Draper, S. Boardsen, and C. Dong, "When the Moon Had a Magnetosphere," Science Advances, vol. 6, no. 42, Oct. 2020, doi: 10.1126/sciadv.abc0865. Available: https://pmc.ncbi.nlm.nih.gov/articles/PMC10763664/

10) A. Cermak, "Mars Exploration - NASA Science," NASA Science, Aug. 01, 2025. Available: https://science.nasa.gov/planetary-science/programs/mars-exploration/

11) "Why Go to Mars?" Available: https://www.esa.int/Science_Exploration/Human_and_Robotic_Exploration/Exploration/Why_go_to_Mars#:~:text=The%20scientific%20reasons%20for%20going%20to%20Ma

rs%20can,beyond%20Earth%20is%20a%20fundamental%20question%20of%20humankind.

12) J. T. Fisher, U. Ciuha, P. Denise, A. C. McDonnell, H. Normand, and I. B. Mekjavic, "The Combined Effects of Artificial Gravity, Temperature, and Hypoxia on Haemodynamic Responses and Limb Blood Flow," European Journal of Applied Physiology, Apr. 2025, doi: 10.1007/s00421-025-05773-7. Available: https://doi.org/10.1007/s00421-025-05773-7

13) S. A. Narayanan, "Gravity's Effect on Biology," Frontiers in Physiology, vol. 14, Jul. 2023, doi: 10.3389/fphys.2023.1199175. Available: https://pmc.ncbi.nlm.nih.gov/articles/PMC10351380/

14) E. R. Morey-Holton, "The Impact of Gravity on Life," in Elsevier eBooks, 2003, pp. 143–159. doi: 10.1016/b978-012598655-7/50036-7. Available: https://www.sciencedirect.com/science/article/pii/B9780125986557500367?via%3Dihub

15) M. L. Lewis et al., "cDNA Microarray Reveals Altered Cytoskeletal Gene Expression in Space-Flown Leukemic T Lymphocytes (Jurkat)," The FASEB Journal, vol. 15, no. 10, pp. 1783–1785, Jun. 2001, doi: 10.1096/fj.00-0820fje. Available: https://pubmed.ncbi.nlm.nih.gov/11481229/

16) N. E. Ward, N. R. Pellis, S. A. Risin, and D. Risin, "Gene Expression Alterations in Activated Human T-cells Induced by Modeled Microgravity," Journal of Cellular Biochemistry, vol. 99, no. 4, pp. 1187–1202, Jan. 2006, doi: 10.1002/jcb.20988. Available: https://pubmed.ncbi.nlm.nih.gov/16795038/

17) T. T. Chang et al., "The Rel/NF-κB Pathway and Transcription of Immediate Early Genes in T Cell Activation Are Inhibited by Microgravity," Journal of Leukocyte Biology, vol. 92, no. 6, pp. 1133–1145, Jul. 2012, doi: 10.1189/jlb.0312157. Available: https://pubmed.ncbi.nlm.nih.gov/22750545/

18) S. Tauber, S. Christoffel, C. S. Thiel, and O. Ullrich, "Transcriptional Homeostasis of Oxidative Stress-Related Pathways in Altered Gravity," International Journal of Molecular Sciences, vol. 19, no. 9, p. 2814, Sep. 2018, doi: 10.3390/ijms19092814. Available: https://pubmed.ncbi.nlm.nih.gov/30231541/

19) E. S. Baker, M. R. Barratt, C. F. Sams, and M. L. Wear, "Human Response to Space Flight," in Springer eBooks, 2019, pp. 367–411. doi: 10.1007/978-1-4939-9889-0_12. Available: https://doi.org/10.1007/978-1-4939-9889-0_12

20) S. Trappe et al., "Exercise in Space: Human Skeletal Muscle After 6 Months Aboard the International Space Station," Journal of Applied Physiology, vol. 106, no. 4, pp. 1159–1168, Jan. 2009, doi: 10.1152/japplphysiol.91578.2008. Available: https://doi.org/10.1152/japplphysiol.91578.2008

21) A. D. Moore, M. E. Downs, S. M. C. Lee, A. H. Feiveson, P. Knudsen, and L. Ploutz-Snyder, "Peak Exercise Oxygen Uptake During and Following Long-Duration

Spaceflight," Journal of Applied Physiology, vol. 117, no. 3, pp. 231–238, Jun. 2014, doi: 10.1152/japplphysiol.01251.2013. Available: https://doi.org/10.1152/japplphysiol.01251.2013

22) J. D. Sibonga, E. R. Spector, S. L. Johnston, and W. J. Tarver, "Evaluating Bone Loss in ISS Astronauts," Aerospace Medicine and Human Performance, vol. 86, no. 12:Supplement, pp. A38–A44, Nov. 2015, doi: 10.3357/amhp.ec06.2015. Available: https://pubmed.ncbi.nlm.nih.gov/26630194/

23) C. Richter, B. Braunstein, A. Winnard, M. Nasser, and T. Weber, "Human Biomechanical and Cardiopulmonary Responses to Partial Gravity – a systematic review," Frontiers in Physiology, vol. 8, Aug. 2017, doi: 10.3389/fphys.2017.00583. Available: https://doi.org/10.3389/fphys.2017.00583

24) NASA, "Apollo 15: Mission Details - NASA," NASA, Sep. 29, 2023. Available: https://www.nasa.gov/missions/apollo/apollo-15-mission-details/

25) C. Richter, B. Braunstein, A. Winnard, M. Nasser, and T. Weber, "Human Biomechanical and Cardiopulmonary Responses to Partial Gravity – a systematic review," Frontiers in Physiology, vol. 8, Aug. 2017, doi: 10.3389/fphys.2017.00583. Available: https://doi.org/10.3389/fphys.2017.00583

26) Apollo11Space, "Apollo Program Costs (New Data 1969 vs 2024)," Apollo11Space, Mar. 17, 2024. Available: https://apollo11space.com/apollo-program-costs-new-data-1969-vs-2024/

27) Apollo11Space, "Apollo Program Failures and Lessons Learned: NASA's Journey to the Moon," Apollo11Space, Aug. 18, 2024. Available: https://apollo11space.com/apollo-program-failures-and-lessons-learned-nasas-journey-to-the-moon/

28) F. E. Garrett-Bakelman et al., "The NASA Twins Study: A Multidimensional Analysis of a Year-Long Human Spaceflight," Science, vol. 364, no. 6436, Apr. 2019, doi: 10.1126/science.aau8650. Available: https://doi.org/10.1126/science.aau8650

29) "Twins Study - NASA," NASA. Available: https://www.nasa.gov/humans-in-space/twins-study/

30) S. Zhang, T. Adachi, S. Zhang, Y. Yoshida, and A. Takahashi, "A New Type of Simulated Partial Gravity Apparatus for Rats Based on a Pully-Spring System," Frontiers in Cell and Developmental Biology, vol. 10, Aug. 2022, doi: 10.3389/fcell.2022.965656. Available: https://pmc.ncbi.nlm.nih.gov/articles/PMC9472129/

31) M. Stephenson and W. Grayson, "Recent Advances in Bioreactors for Cell-Based Therapies," F1000Research, vol. 7, p. 517, Apr. 2018, doi: 10.12688/f1000research.12533.1. Available: https://pmc.ncbi.nlm.nih.gov/articles/PMC5931275/

32) "NASA Bioreactors Advance Disease Treatments | NASA Spinoff." Available: https://spinoff.nasa.gov/Spinoff2009/hm_3.html

33) J. Wong, "Cells in Space," Nature Medicine, vol. 3, no. 3, p. 259, Mar. 1997, doi: 10.1038/nm0397-259b. Available: https://www.nature.com/articles/nm0397-259b

34) The Editors of Encyclopaedia Britannica, "Physical Constant | Definition, Examples & Units," Encyclopedia Britannica, Jul. 20, 1998. Available: https://www.britannica.com/science/physical-constant

35) Hasenstein, K. H., & Van Loon, J. J. W. A. (2022). Clinostats and Other Rotating Systems—Design, Function, and Limitations. In River Publishers eBooks (pp. 147–156). https://doi.org/10.1201/9781003338277-17

36) "Zero Gravity Noun - Definition, Pictures, Pronunciation and Usage Notes | Oxford Advanced Learner's Dictionary at OxfordLearnersDictionaries.com." Available: https://www.oxfordlearnersdictionaries.com/definition/english/zero-gravity

37) Cook, A. H, Nordtvedt, K. L, Faller, and J. E, "Gravity | Definition, Physics, & Facts," Encyclopedia Britannica, Aug. 13, 2025. Available: https://www.britannica.com/science/gravity-physics/Newtons-law-of-gravity

38) J. Sánchez-Haro, I. Lombillo, and G. Capellán, "Simplified Model to Consider Influence of Gravity on Impacts on Structures: Experimental and Numerical Validation," International Journal of Impact Engineering, vol. 173, p. 104474, Dec. 2022, doi: 10.1016/j.ijimpeng.2022.104474. Available: https://www.sciencedirect.com/science/article/pii/S0734743X22003141

39) D. R. Morrison, ed., "Space Bioreactor Science Workshop", Johnson Space Center, Houston, TX; National Aeronautics and Space Administration, Washington, D.C., NASA CP-2485, Aug. 1985. Available: https://archive.org/download/Bioreactor01/bioreactor%2001.pdf.

40) NASA, "What is Microgravity? - NASA," NASA, Jul. 25, 2023. Available: https://www.nasa.gov/centers-and-facilities/glenn/what-is-microgravity/

41) A. Manzano et al., "Novel, Moon and Mars, Partial Gravity Simulation Paradigms and Their Effects on the Balance Between Cell Growth and Cell Proliferation During Early Plant Development," Npj Microgravity, vol. 4, no. 1, Mar. 2018, doi: 10.1038/s41526-018-0041-4. Available: https://www.nature.com/articles/s41526-018-0041-4

42) R. S. Thombre, K. Kaur, S. S. Jagtap, J. Dixit, and P. V. Vaishampayan, "Microbial Life in Space," in New Frontiers in Astrobiology, Elsevier, 2022, pp. 135–166. [Online]. Available: https://www.sciencedirect.com/science/article/abs/pii/B9780128241622000130

43) V. Chantseva, T. Bilova, G. Smolikova, A. Frolov, and S. Medvedev, "3D-Clinorotation Induces Specific Alterations in Metabolite Profiles of Germinating Brassica Napus L.

Seeds," Biological Communications, vol. 64, no. 1, pp. 55–74, Jan. 2019, doi: 10.21638/spbu03.2019.107. Available: https://www.researchgate.net/publication/333850184_3D-clinorotation_induces_specific_alterations_in_metabolite_profiles_of_germinating_Brassica_napus_L_seeds

44) F. J. Medina, A. Manzano, A. Villacampa, M. Ciska, and R. Herranz, "Understanding Reduced Gravity Effects on Early Plant Development Before Attempting Life-Support Farming in the Moon and Mars," Frontiers in Astronomy and Space Sciences, vol. 8, Sep. 2021, doi: 10.3389/fspas.2021.729154. Available: https://www.researchgate.net/publication/354358925_Understanding_Reduced_Gravity_Effects_on_Early_Plant_Development_Before_Attempting_Life-Support_Farming_in_the_Moon_and_Mars

45) B. R. Unsworth and P. I. Lelkes, "Growing Tissues in Microgravity," Nature Medicine, vol. 4, no. 8, pp. 901–907, Aug. 1998, doi: 10.1038/nm0898-901. Available: https://www.nature.com/articles/nm0898-901

46) "United Nations Sustainable Development Goals (SDGs)," UN Regional Information Centre for Western Europe, UNRIC. Available: https://unric.org/en/united-nations-sustainable-development-goals/

47) "Goal 3 | Good Health and Well-Being." Available: https://sdgs.un.org/goals/goal3

48) "Goal 12 | Responsible Consumption and Production." Available: https://sdgs.un.org/goals/goal12

49) F. Palladino et al., "Bioreactors: Applications and Innovations For A Sustainable And Healthy Future—A Critical Review," Applied Sciences, vol. 14, no. 20, p. 9346, Oct. 2024, doi: 10.3390/app14209346. Available: https://www.researchgate.net/publication/384925238_Bioreactors_Applications_and_Innovations_for_a_Sustainable_and_Healthy_Future-A_Critical_Review

50) "Goal 13 | Climate Action." Available: https://sdgs.un.org/goals/goal13

51) "Goal 9 | Industry, Innovation, and Infrastructure." Available: https://sdgs.un.org/goals/goal9

52) "FAQs : The International Space Station Transition Plan - NASA," NASA. Available: https://www.nasa.gov/faqs-the-international-space-station-transition-plan/#q3

53) "Destinations - NASA," NASA. Available: https://www.nasa.gov/humans-in-space/destinations/

54) J. Swanenburg, C. A. Easthope, A. Meinke, A. Langenfeld, D. A. Green, and P. Schweinhardt, "Lunar and Mars Gravity Induce Similar Changes in Spinal Motor Control as Microgravity," Frontiers in Physiology, vol. 14, Jul. 2023, doi:

10.3389/fphys.2023.1196929. Available: https://pmc.ncbi.nlm.nih.gov/articles/PMC10411353/

55) Harland and D. M, "Microgravity | Space Exploration, Astronauts & Zero-Gravity," Encyclopedia Britannica, Nov. 19, 2007. Available: https://www.britannica.com/science/microgravity

56) "Scientists Create Model to Measure How Cells Sense Their Surroundings," ScienceDaily, Mar. 20, 2020. Available: https://www.sciencedaily.com/releases/2020/03/200326144348.htm

57) "Gravity: It's Only a Theory | National Center for Science Education." Available: https://ncse.ngo/gravity-its-only-theory

58) J. Berro, "'Essentially, All Models Are Wrong, But Some Are Useful'—A Cross-Disciplinary Agenda for Building Useful Models in Cell Biology and Biophysics," Biophysical Reviews, vol. 10, no. 6, pp. 1637–1647, Nov. 2018, doi: 10.1007/s12551-018-0478-4. Available: https://pmc.ncbi.nlm.nih.gov/articles/PMC6297095/

59) Nuaire, "NU-5810 High Heat Decontamination CO2 incubator," www.nuaire.com. Available: https://www.nuaire.com/products/co2-incubators/direct-heat/in-vitrocell-nu-5810-direct-heat-decon-co2-incubator

60) "ISO 13850:2015," ISO. Available: https://www.iso.org/standard/59970.html

61) "IEC 61010-2-030:2023," IEC. Available: https://webstore.iec.ch/en/publication/75915

62) Admin, "IEC 60204-1: Safety of Machinery and Electrical equipment Design : Electrical Engineering Hub," Electrical Hub, May 31, 2025. Available: https://azadtechhub.com/iec-60204-1-safety-of-machinery-and-electrical-equipment-design/

63) C.-P. Segeritz and L. Vallier, "Cell Culture," in Elsevier eBooks, 2017, pp. 151–172. doi: 10.1016/b978-0-12-803077-6.00009-6. Available: https://www.sciencedirect.com/science/article/pii/B9780128030776000096

64) Standard Guide for Quantifying Cell Viability and Related Attributes within Biomaterial Scaffolds," ASTM F2739-19, ASTM International, 2019. Available: https://compass.astm.org/document/?contentCode=ASTM%7CF2739-19%7Cen-US&proxycl=https%3A%2F%2Fsecure.astm.org&fromLogin=true

65) A. Simonyan and N. Sarvazyan, "Bioreactors," in Learning materials in biosciences, 2020, pp. 127–136. doi: 10.1007/978-3-030-39698-5_11. Available: https://doi.org/10.1007/978-3-030-39698-5_11

66) M. Stephenson and W. Grayson, "Recent Advances in Bioreactors for Cell-Based Therapies," F1000Research, vol. 7, p. 517, Apr. 2018, doi:

10.12688/f1000research.12533.1. Available: https://pmc.ncbi.nlm.nih.gov/articles/PMC5931275/

67) Fern J. Armistead, Julia Gala De Pablo, Hermes Gadêlha, Sally A. Peyman, Stephen D. Evans, "Cells Under Stress: An Inertial-Shear Microfluidic Determination of Cell Behavior," Biophysical Journal, vol. 116, issue 6, pgs. 1127-1135, 2019, ISSN 0006 3495. Available: https://doi.org/10.1016/j.bpj.2019.01.034

68) C. A. Nickerson, C. M. Ott, J. W. Wilson, R. Ramamurthy, and D. L. Pierson, "Microbial Responses to Microgravity and Other Low-Shear Environments," Microbiology and Molecular Biology Reviews, vol. 68, no. 2, pp. 345–361, Jun. 2004, doi: 10.1128/mmbr.68.2.345-361.2004. Available: https://pmc.ncbi.nlm.nih.gov/articles/PMC419922/

69) D. Nowacki, F. G. Klinger, G. Mazur, and M. De Felici, "Effect of Culture in Simulated Microgravity on the Development of Mouse Embryonic Testes," Advances in Clinical and Experimental Medicine, vol. 24, no. 5, pp. 769–774, Sep. 2015, doi: 10.17219/acem/27920. Available: https://www.researchgate.net/publication/283754366_Effect_of_Culture_in_Simulated_Microgravity_on_the_Development_of_Mouse_Embryonic_Testes

70) H. Andrade-Zaldívar, L. Santos, and A. De León Rodríguez, "Expansion of Human Hematopoietic Stem Cells for Transplantation: Trends and Perspectives," Cytotechnology, vol. 56, no. 3, pp. 151–160, Mar. 2008, doi: 10.1007/s10616-008-9144-1. Available: https://www.researchgate.net/publication/23467300_Expansion_of_human_hematopoietic_stem_cells_for_transplantation_Trends_and_perspectives

71) M. A. Phelan, A. L. Gianforcaro, J. A. Gerstenhaber, and P. I. Lelkes, "An Air Bubble-Isolating Rotating Wall Vessel Bioreactor for Improved Spheroid/Organoid Formation," Tissue Engineering Part C Methods, vol. 25, no. 8, pp. 479–488, Jul. 2019, doi: 10.1089/ten.tec.2019.0088. Available: https://pmc.ncbi.nlm.nih.gov/articles/PMC6686703/?term=%22Tissue%20Eng%20Part%20C%20Methods%22%5Bjour%5D

72) Phelan, M. A. (2018). The design, construction, and validation of novel rotating wall vessel bioreactors (Master's thesis, Temple University). Temple University Graduate Board.

73) Phelan, M. A. (2021). Bioengineering approaches for improved differentiation of cultured retinal tissues from pluripotent stem cells (Doctoral dissertation, Temple University). Temple University Graduate Board.

74) P. R. Cavanagh et al., "A Novel Lunar Bed Rest Analogue," Aviation Space and Environmental Medicine, vol. 84, no. 11, pp. 1191–1195, Oct. 2013, doi: 10.3357/asem.3472.2013. Available: https://pubmed.ncbi.nlm.nih.gov/24279234/

75) G. R. ClÃ©Ment, A. P. Bukley, and W. H. Paloski, “Artificial Gravity as a Countermeasure for Mitigating Physiological Deconditioning During Long-Duration Space Missions,” Frontiers in Systems Neuroscience, vol. 9, Jun. 2015, doi: 10.3389/fnsys.2015.00092. Available: https://www.researchgate.net/publication/279728802_Artificial_gravity_as_a_countermeasure_for_mitigating_physiological_deconditioning_during_long-duration_space_missions

76) “Centripetal Acceleration | Physics.” Available: https://courses.lumenlearning.com/suny-physics/chapter/6-2-centripetal-acceleration/

77) G. Clément, “International Roadmap for Artificial Gravity Research,” Npj Microgravity, vol. 3, no. 1, Nov. 2017, doi: 10.1038/s41526-017-0034-8. Available: https://www.nature.com/articles/s41526-017-0034-8

78) J. L. P. Pavón, S. H. Martín, C. G. Pinto, and B. M. Cordero, “Determination of Trihalomethanes in Water Samples: A Review,” Analytica Chimica Acta, vol. 629, no. 1–2, pp. 6–23, Sep. 2008, doi: 10.1016/j.aca.2008.09.042. Available: https://www.researchgate.net/publication/23402927_Determination_of_trihalomethanes_in_water_samples_A_review

79) A. W. Nienow, B. Isailovic, and T. A. Barrett, “Design and Performance of Single-Use, Stirred-Tank bioreactors,” Jan. 30, 2024. Available: https://www.bioprocessintl.com/single-use/design-and-performance-of-single-use-stirred-tank-bioreactors

80) M. Scholz, “Weighted Decision Matrix: A Tool for Pro-Level Prioritization,” airfocus, Jun. 26, 2025. Available: https://airfocus.com/blog/weighted-decision-matrix-prioritization/

81) “Parabolic flight - NASA,” NASA. Available: https://www.nasa.gov/mission/parabolic-flight/

82) J. J. W. A. Van Loon, “Centrifuges for Microgravity Simulation. The Reduced Gravity Paradigm,” Frontiers in Astronomy and Space Sciences, vol. 3, Jul. 2016, doi: 10.3389/fspas.2016.00021. Available: https://doi.org/10.3389/fspas.2016.00021

83) The Editors of Encyclopaedia Britannica, “Equivalence Principle | Gravitational, Acceleration & Time Dilation,” Encyclopedia Britannica, Jul. 20, 1998. Available: https://www.britannica.com/science/equivalence-principle

84) A. Barzegari and A. A. Saei, “An Update to Space Biomedical Research: Tissue Engineering in Microgravity Bioreactors.,” DOAJ (DOAJ: Directory of Open Access Journals), Jan. 2012, doi: 10.5681/bi.2012.003. Available: https://pmc.ncbi.nlm.nih.gov/articles/PMC3648913/

85) A. L. Radtke and M. M. Herbst-Kralovetz, “Culturing and Applications of Rotating Wall Vessel Bioreactor Derived 3D Epithelial Cell Models,” Journal of Visualized

Experiments, no. 62, Apr. 2012, doi: 10.3791/3868. Available: https://pmc.ncbi.nlm.nih.gov/articles/PMC3567125/

86) J. P. Licata, K. H. Schwab, Y.-E. Har-El, J. A. Gerstenhaber, and P. I. Lelkes, "Bioreactor Technologies for Enhanced Organoid Culture," International Journal of Molecular Sciences, vol. 24, no. 14, p. 11427, Jul. 2023, doi: 10.3390/ijms241411427. Available: https://www.researchgate.net/publication/372622186_Bioreactor_Technologies_for_Enhanced_Organoid_Culture

87) T. J. Goodwin, T. L. Prewett, D. A. Wolf, and G. F. Spaulding, "Reduced Shear Stress: A Major Component in the Ability of Mammalian Tissues to Form Three-Dimensional Assemblies in Simulated Microgravity," Journal of Cellular Biochemistry, vol. 51, no. 3, pp. 301–311, Mar. 1993, doi: 10.1002/jcb.240510309. Available: https://pubmed.ncbi.nlm.nih.gov/8501132/

88) T. G. Hammond and J. M. Hammond, "Optimized Suspension Culture: the Rotating-Wall Vessel," AJP Renal Physiology, vol. 281, no. 1, pp. F12–F25, Jul. 2001, doi: 10.1152/ajprenal.2001.281.1.f12. Available: https://doi.org/10.1152/ajprenal.2001.281.1.f12

89) S. Navran, "The Application of Low Shear Modeled Microgravity to 3-D cell Biology and Tissue Engineering," Biotechnology Annual Review, pp. 275–296, Jan. 2008, doi: 10.1016/s1387-2656(08)00011-2. Available: https://pubmed.ncbi.nlm.nih.gov/18606368/

90) A. Wnorowski et al., "Effects of Spaceflight on Human Induced Pluripotent Stem Cell-Derived Cardiomyocyte Structure and Function," Stem Cell Reports, vol. 13, no. 6, pp. 960–969, Nov. 2019, doi: 10.1016/j.stemcr.2019.10.006. Available: https://pubmed.ncbi.nlm.nih.gov/31708475/

91) P. M. Gershovich, J. G. Gershovich, A. P. Zhambalova, Yu. A. Romanov, and L. B. Buravkova, "Cytoskeletal Proteins and Stem Cell Markers Gene Expression in Human Bone Marrow Mesenchymal Stromal Cells After Different Periods of Simulated Microgravity," Acta Astronautica, vol. 70, pp. 36–42, Sep. 2011, doi: 10.1016/j.actaastro.2011.07.028. Available: https://www.sciencedirect.com/science/article/abs/pii/S0094576511002402

92) N. Yamaguchi et al., "Microbial Monitoring of Crewed Habitats in Space—Current status and Future Perspectives," Microbes and Environments, vol. 29, no. 3, pp. 250–260, Jan. 2014, doi: 10.1264/jsme2.me14031. Available: https://www.researchgate.net/publication/264867408_Microbial_Monitoring_of_Crewed_Habitats_in_Space-Current_Status_and_Future_Perspectives

93) F. Arias et al., "Mars Artificial Gravity Habitat with Centrifugation (MAGICIAN)," IEEE Aerospace Conference, pp. 1–17, Mar. 2024, doi: 10.1109/aero58975.2024.10521126. Available: https://www.researchgate.net/publication/380558478_Mars_Artificial_Gravity_Habitat_with_Centrifugation_MAGICIAN

94) Barnard, R. Walter, Maor, and Eli, "Trigonometry | Definition, Formulas, Ratios, & Identities," Encyclopedia Britannica, Aug. 18, 2025. Available: https://www.britannica.com/science/trigonometry

95) TrueGeometry, "How to Calculate RPM from Angular Velocity In Context of RPM to Angular Velocity," True Geometry's Blog, Sep. 12, 2024. Available: https://blog.truegeometry.com/tutorials/education/b372e069150d103d6263046cc3742829/JSON_TO_ARTCL_How_to_Calculate_RPM_from_Angular_Velocity_in_context_of_rpm_to_an.html

96) A. J. Banko and J. K. Eaton, "Particle Dispersion and Preferential Concentration in Particle-Laden Turbulence," in Elsevier eBooks, 2023, pp. 43–79. doi: 10.1016/b978-0-32-390133-8.00011-6. Available: https://www.sciencedirect.com/topics/physics-and-astronomy/settling-velocity

97) Gregersen and Erik, "Stokes's Law | Definition, Formula, & Facts," Encyclopedia Britannica, Jul. 20, 1998. Available: https://www.britannica.com/science/Stokess-law

98) T. West and A. Photiou, "Measurement of Gas Volume and Gas Flow," Anaesthesia & Intensive Care Medicine, vol. 19, no. 4, pp. 183–188, Mar. 2018, doi: 10.1016/j.mpaic.2018.02.004. Available: https://www.sciencedirect.com/topics/engineering/reynolds-number

99) W. Zhu and H. Obara, "Flow Structure of Okra Mucilage in Rotating Wall Vessel System," Heliyon, vol. 10, no. 16, p. e36149, Aug. 2024, doi: 10.1016/j.heliyon.2024.e36149. Available: https://www.sciencedirect.com/science/article/pii/S2405844024121809

100) J. A. Espina, M. H. Cordeiro, M. Milivojevic, I. Pajić-Lijaković, and E. H. Barriga, "Response of Cells and Tissues to Shear Stress," Journal of Cell Science, vol. 136, no. 18, Sep. 2023, doi: 10.1242/jcs.260985. Available: https://pmc.ncbi.nlm.nih.gov/articles/PMC10560560/

101) M. Ebrahimi, "Extracellular Matrix: The Ideal Natural Fibrous Nanocomposite Products," in Elsevier eBooks, 2018, pp. 263–286. doi: 10.1016/b978-0-12-813740-6.00014-4. Available: https://www.sciencedirect.com/topics/engineering/fluid-shear-stress

102) W. A. Altabey, "Load and Stress Analysis," in Elsevier eBooks, 2024, pp. 7–41. doi: 10.1016/b978-0-443-21449-3.00021-9. Available: https://www.sciencedirect.com/topics/biochemistry-genetics-and-molecular-biology/shear-stress

103) S. Yao, C. Chang, K. Hai, H. Huang, and H. Li, "A Review of Experimental Studies on the Proppant Settling in Hydraulic Fractures," Journal of Petroleum Science and Engineering, vol. 208, p. 109211, Jul. 2021, doi: 10.1016/j.petrol.2021.109211. Available: https://www.sciencedirect.com/topics/engineering/particle-reynolds-number

104) "The Influence of Particles on Suspension Rheology | Anton Paar Wiki," Anton Paar. Available: https://wiki.anton-paar.com/en/the-influence-of-particles-on-suspension-rheology/

105) D. A. Charlebois and G. Balázsi, "Modeling Cell Population Dynamics," In Silico Biology, vol. 13, no. 1–2, pp. 21–39, Dec. 2018, doi: 10.3233/isb-180470. Available: https://pmc.ncbi.nlm.nih.gov/articles/PMC6598210/

106) E. M. Martinez, M. C. Yoshida, T. L. T. Candelario, and M. Hughes-Fulford, "Spaceflight and Simulated Microgravity Cause a Significant Reduction of Key Gene Expression in Early T-Cell Activation," AJP Regulatory Integrative and Comparative Physiology, vol. 308, no. 6, pp. R480–R488, Jan. 2015, doi: 10.1152/ajpregu.00449.2014. Available: https://www.researchgate.net/publication/270659952_Spaceflight_and_simulated_microgravity_cause_a_significant_reduction_of_key_gene_expression_in_early_T-cell_activation

107) L. R. Brewer and P. R. Bianco, "Laminar Flow Cells for Single-Molecule Studies of DNA-Protein Interactions," Nature Methods, vol. 5, no. 6, pp. 517–525, May 2008, doi: 10.1038/nmeth.1217. Available: https://pmc.ncbi.nlm.nih.gov/articles/PMC7141782/

108) K. Yamamoto, Y. Shimogonya, R. Maeno, K. Kawabe, and J. Ando, "Endothelial Cells Differentially Sense Laminar and Disturbed Flows by Altering the Lipid Order of Their Plasma and Mitochondrial Membranes," AJP Cell Physiology, vol. 325, no. 6, pp. C1532–C1544, Nov. 2023, doi: 10.1152/ajpcell.00393.2023. Available: https://pmc.ncbi.nlm.nih.gov/articles/PMC10861177/

109) V. Chatziravdeli, G. N. Katsaras, and G. I. Lambrou, "Gene Expression in Osteoblasts and Osteoclasts Under Microgravity Conditions: A Systematic review," Current Genomics, vol. 20, no. 3, pp. 184–198, Apr. 2019, doi: 10.2174/1389202920666190422142053. Available: https://pmc.ncbi.nlm.nih.gov/articles/PMC6935951/

110) J. Braveboy-Wagner and P. I. Lelkes, "Impairment of 7F2 Osteoblast Function by Simulated Partial Gravity in a Random Positioning Machine," Npj Microgravity, vol. 8, no. 1, Jun. 2022, doi: 10.1038/s41526-022-00202-x. Available: https://pubmed.ncbi.nlm.nih.gov/35672327/

111) J. L. Brown and C. T. Laurencin, "Bone Tissue Engineering," in Biomaterials Science, 2020, pp. 1373–1388. doi: 10.1016/b978-0-12-816137-1.00085-4. Available: https://www.sciencedirect.com/topics/materials-science/osteoblast?utm_source=chatgpt.com

112) G. E. Neurohr and A. Amon, "Relevance and Regulation of Cell Density," Trends in Cell Biology, vol. 30, no. 3, pp. 213–225, Jan. 2020, doi: 10.1016/j.tcb.2019.12.006. Available: https://pmc.ncbi.nlm.nih.gov/articles/PMC8777196/

113) L. E. Bourne and I. R. Orriss, “Isolation and Culture of Osteoblasts,” Methods in Molecular Biology, pp. 3–22, Jan. 2025, doi: 10.1007/978-1-0716-4306-8_1. Available: https://doi.org/10.1007/978-1-0716-4306-8_1

114) C. Poon, “Measuring The Density and Viscosity of Culture Media for Optimized Computational Fluid Dynamics Analysis of In Vitro Devices,” Journal of the Mechanical Behavior of Biomedical Materials/Journal of Mechanical Behavior of Biomedical Materials, vol. 126, p. 105024, Dec. 2021, doi: 10.1016/j.jmbbm.2021.105024. Available: https://www.sciencedirect.com/science/article/pii/S1751616121006500

115) “McMaster-Carr.” Available: https://www.mcmaster.com/6627T56/

116) “McMaster-Carr.” Available: https://www.mcmaster.com/6627T912/

117) “Arduino Uno WiFi Rev2 – ATmega4809, WiFi & Bluetooth, Secure,” Arduino Online Shop. Available: https://store-usa.arduino.cc/products/arduino-uno-wifi-rev2

118) “Physical Properties of Acrylic Sheets,” BuildItSolar, Aug. 2005. https://www.builditsolar.com/References/Glazing/physicalpropertiesAcrylic.pdf

119) D. McClements and P. Keane, “Aluminum: Properties, Uses, and Benefits,” Sep. 22, 2025. Available: https://www.thomasnet.com/articles/metals-metal-products/aluminum/?msockid=3c3cf3cc76bf62613214e651777d63ba

9. Supplementary Data

Supplementary Table S 1: Bioreactor Systems for Cell Expansion

Bioreactor type	Commercial examples	Parameter ranges	Advantages/limitations	Example case studies	References
Rocking bed (wave motion)	• WAVE (GE Healthcare) • Finesse (Thermo Fisher) • Biostat (Sartorius)	• Size (1–500 L) • Rocking angle: 5–35° • Rotation speed: 10–35 rpm	Advantages: • Versatile single-use bags Limitations: • Limited scale-up potential	• Cell type: hMSCs • Method: microcarrier culture • Culture time: 7 days • Fold expansion: 0.7–14.5 • Metrics: viability, tri-lineage differentiation, aggregate size	[1]
Stirred tank	• Mobius (EMD Millipore) • Finesse (Thermo Fisher)	• Size (100 mL–1,000 L) • Impeller power/speed: variable during culture period • Impeller design: updraft or downdraft, single or multiple	Advantages: • Functional at-large volumes: >50 L Limitations: • Shear forces may impact cell viability/differentiation	• Cell type: hMSCs, hASCs, hiPSCs, and murine ovary cell cells • Method: aggregates, microcarriers, and single-cell suspensions • Culture time: 11–17 days • Fold expansion: 25.7–43 • Metrics: viability, aggregate size, and differentiation capacity	[3][4][5][6]
Rotating wall vessels	RCCMAX (Synthecon)	• Size (100 mL–10 L) • Rotational speed: 5–20 rpm • Continuous medium recirculation or	Advantages: • Low turbulence • Can simulate microgravity Limitations: • Effective only at small volumes: <10 L	• Cell type: hMSCs • Method: scaffolds • Culture time: 21 days • Fold expansion: ~39	[7]

Bioreactor type	Commercial examples	Parameter ranges	Advantages/limitations	Example case studies	References
		closed batch system		• Metrics: viability, surface marker expression, and differentiation	
Perfusion bioreactor	• FiberCell (FiberCell Systems) • Quantum Cell Expansion (Terumo BCT)	• Size (100 mL–5 L) • Perfusion: direct (for example, through scaffolds) or indirect (hollow-fiber, encapsulated cells)	Advantages: • Limited turbulence • Can be automated • Compact Limitations: • Shear forces may impact cell viability/differentiation	• Cell type: hMSCs • Method: encapsulation • Culture time: 21 days • Fold expansion: not applicable • Metrics: viability and differentiation	[8][9]
Isolation/expansion automated systems	• G-Rex (Wilson Wolf) • CliniMACs Prodigy (Miltenyi Biotec)	• Size (100 mL) • Degree of automation	Advantages: • Versatile single-use bags • Automated cell isolation, manipulation, and expansion • GMP-compliant Limitations: • Primarily T-cell expansion	• Cell type: human lymphocytes • Method: suspension culture • Culture time: 8–14 days • Fold expansion: 32–63 • Metrics: viability and cell marker evaluation	[10][11]

GMP, good manufacturing practices; hASC, human adipose-derived stem cell; hiPSC, human induced pluripotent stem cell; hMSC, human mesenchymal stem cell.

Supplementary Table S 1 shows a summary of the different types of bioreactors for cell expansion. It includes their commercial examples, parameter ranges, advantages/ limitations, and example case studies [2].

Supplementary Code S 1. Starter Code

The code is found in the following zip file:
https://1drv.ms/f/c/e85d9878566ceed3/EtePZ4W5e2tKlJr-CJFQVH4BJSjhe2gPj4FKIc9JcPFb_g?e=DyV8yK

10. Supplementary Data References

1) A. Shekaran et al., “Biodegradable ECM-coated PCL Microcarriers Support Scalable Human Early MSC Expansion and In Vivo Bone Formation,” Cytotherapy, vol. 18, no. 10, pp. 1332–1344, Aug. 2016, doi: 10.1016/j.jcyt.2016.06.016. Available: https://pubmed.ncbi.nlm.nih.gov/27503763/

2) M. Stephenson and W. Grayson, “Recent Advances in Bioreactors for Cell-Based Therapies,” F1000Research, vol. 7, p. 517, Apr. 2018, doi: 10.12688/f1000research.12533.1. Available: https://pmc.ncbi.nlm.nih.gov/articles/PMC5931275/

3) Tanja A. Grein, Jasmin Leber, Miriam Blumenstock, Florian Petry, Tobias Weidner, Denise Salzig, Peter Czermak, "Multiphase Mixing Characteristics in a Microcarrier-Based Stirred Tank Bioreactor Suitable for Human Mesenchymal Stem Cell Expansion", Process Biochemistry,vol. 51, issue 9,pgs 1109-1119,2016,ISSN 1359-5113. Available: https://doi.org/10.1016/j.procbio.2016.05.010

4) D. C. Surrao et al., “Large-Scale Expansion of Human Skin-Derived Precursor Cells (hSKPs) in Stirred Suspension Bioreactors,” Biotechnology and Bioengineering, vol. 113, no. 12, pp. 2725–2738, Jun. 2016, doi: 10.1002/bit.26040. Available: https://pubmed.ncbi.nlm.nih.gov/27345530/

5) T. Lawson et al., “Process Development for Expansion of Human Mesenchymal Stromal Cells in a 50L Single-Use Stirred Tank Bioreactor,” Biochemical Engineering Journal, vol. 120, pp. 49–62, Nov. 2016, doi: 10.1016/j.bej.2016.11.020. Available: https://www.sciencedirect.com/science/article/pii/S1369703X16303266

6) S. Markert and K. Joeris, “Establishment of a Fully Automated Microtiter Plate-Based System for Suspension Cell Culture and its Application for Enhanced Process Optimization,” Biotechnology and Bioengineering, vol. 114, no. 1, pp. 113–121, Jul. 2016, doi: 10.1002/bit.26044. Available: https://pubmed.ncbi.nlm.nih.gov/27399304/

7) M. C. Varley, A. E. Markaki, and R. A. Brooks, “Effect of rotation on scaffold motion and cell growth in rotating bioreactors,” Tissue Engineering Part A, vol. 23, no. 11–12, pp. 522–534, Jan. 2017, doi: 10.1089/ten.tea.2016.0357. Available: https://pubmed.ncbi.nlm.nih.gov/28125920/

8) B. B. Nguyen, H. Ko, and J. P. Fisher, “Tunable Osteogenic Differentiation of hMPCs in Tubular Perfusion System Bioreactor,” Biotechnology and Bioengineering, vol. 113, no. 8, pp. 1805–1813, Jan. 2016, doi: 10.1002/bit.25929. Available: https://pubmed.ncbi.nlm.nih.gov/26724678/

9) O. Ball, B.-N. B. Nguyen, J. K. Placone, and J. P. Fisher, “3D printed vascular networks enhance viability in High-Volume perfusion bioreactor,” Annals of Biomedical

Engineering, vol. 44, no. 12, pp. 3435–3445, Jun. 2016, doi: 10.1007/s10439-016-1662-y. Available: https://pubmed.ncbi.nlm.nih.gov/27272210/

10) U. Mock et al., "Automated Manufacturing of Chimeric Antigen Receptor T Cells for Adoptive Immunotherapy Using CliniMACS Prodigy," Cytotherapy, vol. 18, no. 8, pp. 1002–1011, Jul. 2016, doi: 10.1016/j.jcyt.2016.05.009. Available: https://pubmed.ncbi.nlm.nih.gov/27378344/

11) C. Priesner et al., "Automated Enrichment, Transduction, and Expansion of Clinical-Scale CD62L+ T cells for Manufacturing of Gene Therapy Medicinal Products," Human Gene Therapy, vol. 27, no. 10, pp. 860–869, Aug. 2016, doi: 10.1089/hum.2016.091. Available: https://pubmed.ncbi.nlm.nih.gov/27562135/